Solution adsorption formation of a π-conjugated polymer/graphene composite for high-performance field-effect transistors

Liu, Yun; Hao, Wei; Yao, Huiying; Li, Shuzhou; Wu, Yuchen; Zhu, Jia; Jiang, Lei

2017

Liu, Y., Hao, W., Yao, H., Li, S., Wu, Y., Zhu, J., & Jiang, L. (2018). Solution adsorption formation of a π-conjugated polymer/graphene composite for high-performance field-effect transistors. Advanced Materials, 30(3), 1705377-. doi:10.1002/adma.201705377

https://hdl.handle.net/10356/92426

https://doi.org/10.1002/adma.201705377

DOI: 10.1002/ ((please add manuscript number))
Article type: Communication

Solution adsorption formation of a π-conjugated polymer/graphene composite for high-performance field effect transistors

Yun Liu, Wei Hao, Huiying Yao, Jia Zhu, Shuzhou Li, Yuchen Wu, Lei Jiang**

Dr. Y. Liu
Beijing National Laboratory for Molecular Sciences (BNLMS), Key Laboratory of Green Printing, Institute of Chemistry, Chinese Academy of Sciences, Beijing 100190, P. R. China

Dr. Y. C. Wu, Prof. L. Jiang
Key Laboratory of Bio-inspired Materials and Interfacial Science, Technical Institute of Physics and Chemistry, Chinese Academy of Sciences, Beijing 100190, China. Email: wuyuchen@iccas.ac.cn, jianglei@iccas.ac.cn

Dr. H. Y. Yao, Prof. J. Zhu
Department of Chemistry, Beijing Normal University, Beijing 100875, China.

Dr. W. Hao, Prof. S. Z. Li
School of Material Science and Engineering, Nanyang Technological University, Singapore 639798.

Prof. L. Jiang
School of Chemistry and Environment, Beihang University, Beijing 100191, China.

Keywords: π-π interaction, organic semiconductors, graphene, solution adsorption, field-effect-transistors

Abstract

Semiconducting polymers with π-conjugated electronic structures have potential application in the large-scale printable fabrication of high-performance electronic and optoelectronic devices. However, owing to their poor environmental stability and high-cost synthesis, polymer semiconductors possess limited device implementation. Here, we provide an approach for constructing a π-conjugated polymer/graphene composite material to circumvent these limitations and then pattern this material into one-dimensional (1D) arrays. Driven by the π-π interaction, several-layer polymers can be adsorbed onto the graphene planes. The low consumption of the high-cost semiconductor polymers and the mass production of graphene contribute to the low-cost fabrication of the π-conjugated polymer/graphene

composite materials. Based on the π-conjugated system, a reduced π-π stacking distance between graphene and the polymer can be achieved, yielding enhanced charge-transport properties. Owing to the incorporation of graphene, the composite material showed improved thermal stability. More generally, we believe that the construction of π-conjugated composite shows clear possibility of integrating organic molecules and two-dimensional materials into microstructure arrays for property-by-design fabrication of functional devices with large area, low cost and high efficiency.

Semiconducting conjugated polymers possess the unique advantages of designable optoelectronic properties, low-cost solution processability and mechanical flexibility and thus have potential applications in printable integrated circuits,[1-5] wearable sensors, [6-10] and large-area photovoltaic devices.[11,12] Over the last few decades, much effort has been devoted to the optimization of the device configuration, molecular design and synthesis, which has led to the improved performance of polymer-based devices. However, the relatively low charge-carrier mobility, poor environmental stability and large quantities consumed have restricted their practical applications. Integrating polymer semiconductors with high-performance conductors, such as graphene, have provided an effective and facile approach to circumvent these restrictions.[13,14] Owing to the intrinsic high electrical conductivity and thermal stability of graphene, the introduction of graphene has the possibility of improving device performance.[15,16]

Recently, research into graphene-based polymer composites has primarily focused on graphene-filled polymer composites, in which individual graphene sheets are incorporated as fillers in the polymer matrix,[17,18] and graphene functions as an electrically conducting bridge between the polymer domains in the composites. Graphene-filled polymer composites are commonly prepared by solution mixing,[19] melt blending,[20] and in situ polymerization.[21] However, the homogeneous dispersion of graphene in the polymer matrix is relatively

difficult to obtain owing to the unavoidable restacking and aggregation of graphene, thus limiting the mechanical, electrical and thermal performance of the composites. We speculate that the π-electron plane of graphene permits directly adsorption of semiconducting organic molecules by π-π interactions.[15,22-25] Through this approach, several layers of molecules adsorbed onto graphene leads to low consumption of polymers and improved device performance. To further promote these π-conjugated polymer/graphene composite materials into practical electronic devices, a scaled-up assembly technique is prerequisite for fabricating microstructure arrays/patterns.[26-28]

In this work, a π-conjugated polymer/graphene composite material was fabricated by constructing several-layer polymer molecules onto graphene through a solution adsorption process. These materials were further assembled into 1D structures with the guidance of a micropillar-structured template, yielding strictly aligned, highly positioned arrays. A typical p-type donor-acceptor copolymer, poly[2,6-(4,4-bis-alkyl-4H-cyclo-penta-[2,1-b;3,4-b0]-dithiophene)-alt-4,7-(2,1,3-enzothiadia-zole)] (cyclopentadithiophene-benzothiadiazole; CDTBTZ),[29-32] was selected to interact with graphene. The organic field-effect transistor (OFET) devices based on the 1D composite structures showed an average hole mobility of 8.48 $cm^2V^{-1}s^{-1}$. In addition, the composites exhibited enhanced thermal stability. Furthermore, poly(3-hexylthiophene) (P3HT) and poly(3,3-didodecylquaterthiophene) (PQT-12) were successfully composite with graphene. Our results provide a promising method for fabricating solution-processed, high-performance and low-cost organic electronics.

We realized a polymer-graphene conjugated system with several-layer semiconducting polymer adsorbed onto the plane of graphene by employing a solution-processing method. First, the semiconducting polymer CDTBTZ was dissolved into 1,2-dichlorobenzene, followed by the addition of graphene (**Figure 1**a). By blending graphene and the polymer, the polymer was adsorbed onto the graphene planes to construct a polymer-graphene conjugated system, which is dominated by the π-π interactions (Figure 1b). The redundant polymer was

removed through several cycles of vacuum filtration and washing with solvents (Figure 1c and d), yielding the adsorption of several-layer polymers onto the graphene planes (Figure 1e). The inset shows a photograph of the π-conjugated polymer/graphene composite material on a filter. This polymer/graphene composite material can be redispersed into solvent for subsequent device fabrication (Figure 1f). The UV-vis absorption spectra confirm the successful interaction between CDTBTZ and graphene (Figure 1g). Additional UV-vis absorption spectra of the CDTBTZ/graphene composited membrane with different mass ratios and CDTBTZ solutions with different concentrations are shown in Supporting Information Figure S1 and S2. Microscopic Fourier transform infrared spectroscopy (Micro-FTIR) was carried out to confirm the presence of CDTBTZ on graphene after π-π interactions. As shown in Figure 1h, two stretching bands are observed at 2920 cm^{-1} and 2852 cm^{-1}, which can be assigned to the signals of CDTBTZ. The successful conjugation between graphene and P3HT/PQT-12 was also demonstrated by Micro-FTIR spectroscopy (Figure S3 and S4). Furthermore, the electronic energy levels of the polymer and polymer/graphene composite were evaluated by cyclic voltammetry (CV). The levels of the highest occupied molecular orbital (HOMO) and the lowest unoccupied molecular orbital (LUMO) were estimated by the onset of the oxidation and reduction peaks, respectively. As shown in Figure 1g, the bandgap of CDTBTZ of 1.78 eV decreased to 1.22 eV in the CDTBTZ/graphene composite. Besides CDTBTZ, other polymers, such as P3HT and PQT-12, also showed lower bandgaps in the polymer-graphene conjugated system than those in the polymer-polymer system (Figure S3e and Figure S4e).

To integrate the π-conjugated polymer/graphene composite materials into micropatterns for device applications, a capillary-bridge mediated assembly technique was employed using a line-shaped micropillar-structured template (Figure S5). The methodology of this technique relies on the generation of capillary bridges between the target substrate and the tops of the micropillars to control the dewetting of a liquid film. Before performing the assembly

experiments, the micropillar-structured template was modified to have an asymmetric wettability: the top regions of the micropillars were lyophilic, whereas the sidewall and gap regions were lyophobic. This asymmetric wettability was realized by a selective modification process (Figure S6, Supporting Information).[33,34] Briefly, the top regions were selectively protected followed by the low-surface-energy modification of the sidewalls and gaps using heptadecafluorodecyltrimethoxysilane (FAS). After removing the protective layer, the micropillar-structured template with lyophilic tops and lyophobic sidewalls and gaps was generated.

The functional 1D arrays were assembled by dropping a dispersion of the CDTBTZ/graphene composite material onto the micropillar-structured template with asymmetric wettability, which was then covered by a flat substrate to generate a "sandwich-shaped" assembly system (**Figure 2**a). To fully understand the underlying mechanism of the capillary-bridge mediated assembly technique, the dewetting and assembly of the polymer/graphene composite were in-situ observed under an optical microscope. The fluorescence dye 1,5-diaminoanthraquinone was added into the dispersion to observe the assembly process under dark field. Owing to the lyophilic nature of the top regions of the micropillars, the liquid formed a continuous liquid film sandwiched between the flat substrate and the micropillar-structured template (Figure 2b, e and Figure S7a). The quantity of the liquid reduced with the gradual evaporation of the organic solvent. Finally, the liquid film ruptured and divided into regular liquid domain arrays under the guidance of the micropillars. Owing to the asymmetric wettability of the micropillars, the lyophilic top regions served as highly adhesive sites to anchor the liquids, thus forming individual capillary bridges pinned onto the tops of the micropillars (Figure 2c, f and Figure S7b). Following the dewetting of the capillary bridges, the triphase contact line receded, and the size of the capillary bridge decreased. After total evaporation of the organic solvents, 1D assemblies of the polymer/graphene composite were fabricated onto the target substrate with controlled position

and alignment (Figure 2d, g and Figure S7c). The inset above Figure 2d shows the layer-by-layer configuration of the polymer/graphene composite. Therefore, the capillary-bridge mediated assembly technique is a highly effective method, which allows for the large-scale assembly of microstructures onto different substrates for device applications (Figure S8).

In order to investigate the morphology of the aligned 1D arrays, we performed scanning electron microscopy (SEM). From the SEM image shown in Figure 2h, patterned 1D structures of the CDTBTZ/graphene composite are uniform and precisely positioned. The gaps between neighbouring 1D stripes are homogeneous at *ca.* 5 μm, which is consistent with the pillar spacing of the template. A wrinkled and crumpled surface morphology can be observed in the magnified SEM image of an individual 1D structure (Figure 2i). In addition, the regular pattern of CDTBTZ not conjugated to graphene is shown in Figure S9. To demonstrate the wide range of the π-π interaction engineering technique, other conjugated polymers, such as P3HT and PQT-12, were assembled with graphene into 1D arrays through π-π interactions (more details can be found in Figure S3 and S4).

To characterize the precisely positioned 1D CDTBTZ/graphene composite arrays, Raman mapping was carried out. The Raman image shown in Figure 2j, k was collected by mapping the intensity of Raman scattering, with peaks centered at 850 cm^{-1} and 1580 cm^{-1}, which can be attributed to CDTBTZ and graphene, respectively (Figure 2l). The results demonstrate the homogeneous distribution of CDTBTZ on graphene, which confirms the successful fabrication of the polymer/graphene composite. The blue regions show that the gaps were CDTBTZ- and graphene-free, which indicates the successful fabrication of 1D CDTBTZ/graphene composite arrays.

Large-scale, regularly patterned 1D structures of the CDTBTZ/graphene composite were fabricated onto a flat Si wafer containing a 300 nm-thick SiO_2 layer that was modified with octadecyltrichlorosilane (OTS) as a dielectric layer. Then, gold electrodes were evaporated onto the as-prepared 1D arrays as source and drain electrodes, yielding a bottom-gate top-

contact FET. The representative optical micrograph illustrates the structure of the 1D polymer/graphene composite between a pair of metal electrodes (**Figure 3**a). The device configuration and stacking of the polymer/graphene composite in the device are shown in Figure 3b. To evaluate the carrier mobility and on/off ratio of the as-prepared FET devices, over 50 FET devices were measured. Typical transfer and output curves of an FET based on the 1D CDTBTZ/graphene composite arrays are shown in Figure 3c and 3d, displaying an average hole mobility (μ) of 8.48 $cm^2V^{-1}s^{-1}$ (ranging from 6.83 to 9.78 $cm^2V^{-1}s^{-1}$) and on/off current ratio of 10^4. The control device based on 1D CDTBTZ arrays displayed an average mobility of 7.66 $cm^2V^{-1}s^{-1}$ (ranging from 5.72 to 9.46 $cm^2V^{-1}s^{-1}$) and on/off current ratio of 10^4 (Figure 3e, f). The average hole mobilities of the CDTBTZ/graphene composite and CDTBTZ calculated from 50 OFET devices are shown in Figure 3g. The results reveal that improved performance could be achieved through the π-π stacking of graphene and CDTBTZ. Additionally, the representative curves of the temperature dependent carrier mobility over a temperature range of 30 ^oC to 210 ^oC was illustrated in Figure 3h. The mobility of pristine CDTBTZ was falling down over 100 ^oC, which may arose from the changes of crystallinity degree in high temperatures. After the incorporation of graphene, the polymer-graphene conjugated system showed enhanced thermal stability compared with that of the polymer-polymer system, which contributes to its potential applications. Furthermore, slow degradation can be observed in the polymer-graphene conjugated composites when temperature over 150 ^oC, which may contributed by the aggrgation of the subsequent polymer layers over high temperatures except for the first few polymer layer adsorbed on graphene. Besides CDTBTZ, similar results were observed with the other two polymer-graphene-based FETs, as compared to the corresponding polymer-based FETs (Figure S10 and S11), and the devices also showed enhanced thermal stability (Figure S12 and S13).

To reveal the underlying mechanism of the enhanced charge-transport performance, we compared the π-π stacking parameters of the polymer-polymer system and polymer-graphene

conjugated system through grazing-incidence wide-angle X-ray scattering (GIWAXS) and density functional theory (DFT) calculations. Through comparing the GIWAXS results of graphene (Figure S14), the polymer (**Figure 4**a) and the polymer/graphene composite (Figure 4e), the π-π stacking distances can be determined. For graphene, a Q_z value of 1.64 Å^{-1} was observed, corresponding to the distance of 3.83 Å, which can be assigned to the interlayer distance of graphene (Figure S14). The improved interlayer distance of few-layer graphene compared with graphite (3.4 Å) may be induced by oxidation, exfoliation and reduction in the production of graphene.[35] For the polymer, a distance of 3.63 Å was calculated from the diffraction rings lying on the Q_{xy} axis (**Figure 4**a), which can be attributed to the π-π stacking distance of the polymer molecules with edge-on packing configuration (Figure 4b).[30] Under this packing configuration, the π-π stacking orientation is parallel to the charge-transport direction, which is beneficial to electrical conduction and achieving high carrier mobility. Figure 4c shows the π-π stacking distance from the direction parallel to the plane of the thiophene ring. In the polymer-graphene conjugated system, a series of diffraction rings was observed with Q_z values of 2.08, 2.03, 1.68, 1.43, 1.26 Å^{-1} (Figure 4e). By comparing the diffraction results of the polymer and graphene systems, the distances of 3.02 and 3.10 Å mainly along the Q_z axis were observed, which are contributed by π-π stacking between graphene and the polymer. Owing to the lower π-π stacking distance between graphene and polymers, we speculate that the carrier transport process might be dominated by the fast charge transfer from polymer to graphene and efficient conduction in π plane of graphene (illustrated in Figure 4f), which represents a higher-performance transport channel than the intermolecular hopping in pure polymer system. Figure 4g shows the π-π stacking distance from the direction parallel to the plane of the thiophene ring. Obvious changes of packing configuration and distance indicate successful π-π stacking between graphene and the polymer molecules. The possible charge-transport route in the polymer-graphene conjugated system is illustrated in Figure 4d, different from the hopping conduction in polymer-polymer system,

the incorporation of graphene induces a vertical charge transport between graphene and polymers. Charge would transport from the polymer to graphene initially, followed by transport along the two-dimensional π-electron system of graphene. The equivalent circuit of the transport route shown in Figure 4d is illustrated in Figure 4h. Owing to the limited lateral size of the graphene sheets, the polymer adsorbed on the graphene sheets provides a route for charge-carrier transport between the graphene sheets that is faster and shorter than that in the polymer-polymer system.

To compare π-π interactions in the polymer-polymer and polymer-graphene conjugated systems, we employed DFT methods to determine the optimized molecular packing configurations, π-π stacking distances, and electron-ion interactions (details of the calculations are provided in the Experimental section). To simplify the calculation models, the polymer chains were replaced by monomers, and the long alkyl chains were substituted with methyl groups. To study π-π interactions in the polymer-polymer system, four possible molecular packing configurations of two monomers of CDTBTZ were calculated (Figure S15). Their binding energies were calculated to evaluate the stability of the four packing configurations. In the most stable configuration, which had a binding energy of 0.564 eV, the minimum distance and average distance between the conjugated backbones were calculated to be 3.286 Å and 3.396 Å, respectively, using the calculation method shown in Figure S16. After conjugating with graphene (Figure S17), the binding energy between the CDTBTZ monomer and graphene increased to 0.770 eV, indicating stronger π-π interactions between the conjugated organic molecules and delocalized π-system of graphene. The bandgap energies of the CDTBTZ-methyl dimer calculated by DFT decreased in the CDTBTZ monomer/graphene composite, and the HOMO and LUMO diagrams in the two systems are shown in Figure S18. The minimum π-π stacking distance decreased to 3.122 Å, while the average distances in the two systems are very close (Table S1). Reduced π-π stacking distances with a larger overlap area are favourable for charge transport integral and greatly

increase the carrier mobilities when applied to FET devices.[36,37] The results were also confirmed by DFT calculation in the Gaussian09 program package (Figure S19-S21 and Table S2).

In conclusion, we fabricated 1D polymer/graphene composite arrays through π-π interactions via the described method to realizing a system with high carrier mobility and improved thermal stability. With the assistance of a micropillar-structured template and micropillars with asymmetric wettability, regular 1D arrays composed of graphene and conjugated polymers were fabricated. Owing to the existence of graphene and the highly regular molecular chain alignment of the polymers, the conjugated polymer-graphene-based FETs exhibited an increased mobility compared with that based on conjugated polymers. Our approach for fabricating large-area 1D polymer/graphene composite arrays affords low-cost manufacture of organic electronics with high performance and thermal stability.

Experimental section

Fabrication of micropillar structured templates: Silicon wafers (10 cm in diameter, N doped, < 100 > oriented, 525 μm in thickness) were structured by a direct laser-writing apparatus (Heidelberg DWL200) that transferred the computer predefined design onto the photoresist (Shipley Microposit S1800 series)-coated wafer with about 1 μm precision. The patterns of photo-resist formed after irradiation, followed by deep reactive-ion etching (DRIE, Alcatel 601 E) with fluorine-based reagents for various times (10 s-6 min) depending on the desired height of the structures. By designing different photo-masks, pillar-structured silicon wafer with tunable pillar top areas, pillar gaps and pillar top shapes could be fabricated. After resist stripping (Microposit Remover 1165), the substrates were cleaned using ethanol and acetone prior to use.

Preparation of a homogeneous dispersion of the CDTBTZ/graphene composite: The conjugated polymer CDTBTZ was dissolved in ortho-dichlorobenzene to form a homogeneous blue liquid, followed by immersing the graphene sheets into the dilute solution for several hours to ensure full contact. Then, the material was filtered and drip washed with ortho-dichlorobenzene to remove redundant conjugated polymer, leaving several-layer conjugated polymers on the graphene plane. The resultant powder was redispersed in organic solvent with ultrasonication, resulting in a relatively homogeneous dispersion of the conjugated polymer/graphene composite.

Generation of aligned 1D CDTBTZ/graphene composite arrays: A line-shaped micropillar-structured template with a width of 2 μm, separation of 5 μm and depth of 20 μm was employed to guide the dewetting process for the formation of precisely aligned 1D CDTBTZ/graphene composite arrays. A 10 μL droplet of the homogeneous conjugated CDTBTZ/graphene composite dispersion was dropped onto the micropillar-structured template and covered by the desired flat substrate, yielding a sandwich-configuration assembly system. Finally, a 1D dispersion of the conjugated polymer/graphene composite

arrays formed on the target substrate after complete evaporation of the solvent.

Fabrication and measurement of the OFET: OFET devices were fabricated in the bottom-gate and top-contact configuration, and Au was used as the source and drain electrodes. A heavily doped, n-type Si wafer containing a 300 nm-thick SiO_2 layer was used as the substrate. The substrate was washed sequentially with deionized water, hot H_2SO_4:H_2O_2 (7:3) solution, deionized water and isopropyl alcohol and then blown dry using a nitrogen gun. Then, the wafer was cleaned by O_2 plasma to remove organic compounds on the surface and dried under vacuum at 90 °C for 1 h to eliminate any moisture. After cooling to room temperature, a small drop of octadecyltrichlorosilane (OTS) was placed near the wafer. Then, this system was heated to 200 °C and maintained for 2 h under vacuum. The OTS-modified SiO_2/Si wafer was cleaned with n-hexane, trichloromethane and isopropyl alcohol and finally dried under a stream of nitrogen prior to use. The aligned 1D CDTBTZ/graphene composite arrays were generated on the substrate by this pretreatment. The source-drain (S-D) electrodes were thermally evaporated onto the as-prepared 1D arrays through a shadow mask. The electrical characteristics of the OFET devices were measured using a Keithley 4200 SCS semiconductor parameter analyser. All measurements were performed at room temperature in air. The charge-carrier mobility was extracted from the equation:

$$\mu = \frac{2L}{WC_i}\left(\frac{\partial\sqrt{I_{SD}}}{\partial V_G}\right)^2$$

where L and W are the device channel length and width, respectively, I_{SD} is the current between the source and drain electrodes, C_i is the gate capacitance per unit area, and V_G is the gate voltage.

Characterization: The structures of the micropillar-structured template and the morphology of the aligned 1D CDTBTZ/graphene composite arrays were investigated by scanning electron microscopy (SEM, Hitachi, S-4800, Japan) at an accelerating voltage of 5.0 kV and beam current of 10 μA. Raman mapping of the 1D CDTBTZ-graphene conjugate arrays were

measured using a DXR Raman microscope (Thermal Fisher Scientific Inc., USA). Optical and fluorescence micrographs of the aligned 1D CDTBTZ/graphene composite arrays were obtained using an optical microscope (Vision Engineering Co., UK) coupled to a charge-coupled device (CCD) camera and connected to a desktop computer. Infrared spectroscopy was performed after scanning the samples 32 times using a Bruker EQUINOX 55 spectrometer (resolution: 4 cm^{-1}). Grazing-incidence wide-angle X-ray scattering (GIWAXS) patterns were measured on a XEUSS SAXS/WAXS system at an incident angle of 0.2°. Cyclic voltammetry was performed on a CHI660C electrochemistry station. Tetra-butylammonium hexafluorophosphate (Bu_4NPF_6) was used as the supporting electrolyte (0.001 M in dry CH_2Cl_2). Glassy carbon, Pt wire and Ag/AgCl were used as the working, counter and reference electrodes, respectively. Thermogravimetric analysis (TGA) was carried out using a thermoanalyser at a linear heating rate of 10 °C/min under nitrogen flow. Temperature-dependent OFET measurements were performed directly in air with the temperature regulated at a constant heating rate.

DFT calculations: DFT calculations, performed using the Vienna *ab initio* simulation package (VASP),[38] revealed a shorter π-π stacking distance and closer packing in the polymer-graphene conjugated system. The projector augmented wave (PAW)[39] method was used to describe the electron-ion interactions, and the exchange-correlation between electrons was described by the local density approximation (LDA) using the M06L functional,[40] which has been demonstrated to be more accurate to capture the weak dispersion effect between polymers and graphene. We used a cutoff energy of 500 eV for the plane-wave basis set. A (4×12) supercell of a 4-atom graphene unit cell, containing 192 carbon atoms, was used to examine the adsorption of the CDTBTZ monomer on graphene. A 20 Å vacuum was added between the graphene sheets, which is thick enough to safely ignore interlayer graphene interactions. All atoms in the supercell were relaxed until the forces on each atom converged to less than 10^{-2} eV $Å^{-1}$. DFT calculations performed in the Gaussian09 program package also

confirmed the same results. The B3LYP functional combined with the 6-31G(d,p) basis set was adopted for the optimization of the CDTBTZ monomer. The M06L functional in conjunction with the 6-31G(d) basis set was adopted to optimize the configurations of the CDTBTZ dimer and the CDTBTZ monomer adsorbed on graphene.[41]

Supporting Information

Supporting Information is available from the Wiley Online Library or from the author.

Acknowledgements

The authors acknowledge National Research Fund for Fundamental Key Projects (2013CB933000), the National Natural Science Foundation (21421061, 21431009, 21434009, 21504098, 61227902), the Key Research Program of the Chinese Academy of Sciences (KJZD-EW-M03) and the 111 project (B14009).

Received: ((will be filled in by the editorial staff))
Revised: ((will be filled in by the editorial staff))
Published online: ((will be filled in by the editorial staff))

[1] T. Sekitani, U. Zschieschang, H. Klauk, T. Someya, *Nat. Mater.* **2010**, 9, 1015.

[2] B. Crone, A. Dodabalapur, Y. Y. Lin, R. W. Filas, Z. Bao, A. LaDuca, R. Sarpeshkar, H. E. Katz, W. Li, *Nature* **2000**, 403, 521.

[3] H. Sirringhaus, N. Tessler, R. H. Friend, *Science* **1998**, 280, 1741.

[4] Y. Y. Noh, N. Zhao, M. Caironi, H. Sirringhaus, *Nat. Nanotechnol.* **2007**, 2, 784.

[5] C. J. Drury, C. M. J. Mutsaers, C. M. Hart, M. Matters, D. M. de Leeuw, *Appl. Phys. Lett.* **1998**, 73, 108.

[6] G. Schwartz, B. C. K. Tee, J. G. Mei, A. L. Appleton, D. H. Kim, H. L. Wang, Z. N. Bao, *Nat. Commun.* **2013**, 4, 1859.

[7] H. H. Chou, A. Nguyen, A. Chortos, J. W. F. To, C. Lu, J. G. Mei, T. Kurosawa, W. G. Bae, J. B. H. Tok, Z. A. Bao, *Nat. Commun.* **2015**, 6, 8011.

[8] B. C. K. Tee, C. Wang, R. Allen, Z. N. Bao, *Nat. Nanotechnol.* **2012**, 7, 825.

[9] L. J. Pan, A. Chortos, G. H. Yu, Y. Q. Wang, S. Isaacson, R. Allen, Y. Shi, R. Dauskardt, Z. N. Bao, *Nat. Commun.* **2014**, 5, 3002.

[10] O. Knopfmacher, M. L. Hammock, A. L. Appleton, G. Schwartz, J. G. Mei, T. Lei, J. Pei, Z. N. Bao, *Nat. Commun.* **2014**, 5, 2954.

[11] J. Y. Kim, K. Lee, N. E. Coates, D. Moses, T. Q. Nguyen, M. Dante, A. J. Heeger, *Science* **2007**, 317, 222.

[12] H. Y. Chen, J. H. Hou, S. Q. Zhang, Y. Y. Liang, G. W. Yang, Y. Yang, L. P. Yu, Y. Wu, G. Li, *Nat. Photon.* **2009**, 3, 649.

[13] S. Stankovich, D. A. Dikin, G. H. B. Dommett, K. M. Kohlhaas, E. J. Zimney, E. A. Stach, R. D. Piner, S. T. Nguyen, R. S. Ruoff, *Nature* **2006**, 442, 282.

[14] X. D. Zhuang, Y. Chen, G. Liu, P. P. Li, C. X. Zhu, E. T. Kang, K. G. Neoh, B. Zhang, J. H. Zhu, Y. X. Li, *Adv. Mater.* **2010**, 22, 1731.

[15] D. W. He, Y. A. Zhang, Q. S. Wu, R. Xu, H. Y. Nan, J. F. Liu, J. J. Yao, Z. L. Wang, S. J. Yuan, Y. Li, Y. Shi, J. L. Wang, Z. H. Ni, L. He, F. Miao, F. Q. Song, H. X. Xu, K. Watanabe, T. Taniguchi, J. B. Xu, X. R. Wang, *Nat. Commun.* **2014**, 5, 5162.

[16] J. R. Potts, D. R. Dreyer, C. W. Bielawski, R. S. Ruoff, *Polymer* **2011**, 52, 5.

[17] C. J. Lin, C. L. Liu, W. C. Chen, *J. Mater. Chem. C* **2015**, 3, 4290.

[18] H. Kim, A. A. Abdala, C. W. Macosko, *Macromolecules* **2010**, 43, 6515.

[19] T. Ramanathan, A. A. Abdala, S. Stankovich, D. A. Dikin, M. Herrera-Alonso, R. D. Piner, D. H. Adamson, H. C. Schniepp, X. Chen, R. S. Ruoff, S. T. Nguyen, I. A. Aksay, R. K. Prud'homme, L. C. Brinson, *Nat. Nanotechnol.* **2008**, 3, 327.

[20] H. B. Zhang, W. G. Zheng, Q. Yan, Y. Yang, J. W. Wang, Z. H. Lu, G. Y. Ji, Z. Z. Yu, *Polymer* **2010**, 51, 1191.

[21] B. W. Maynor, S. F. Filocamo, M. W. Grinstaff, J. Liu, *J. Am. Chem. Soc.* **2002**, 124, 522.

[22] W. H. Lee, J. Park, S. H. Sim, S. Lim, K. S. Kim, B. H. Hong, K. Cho, *J. Am. Chem. Soc.* **2011**, 133, 4447.

[23] X. L. Liu, X. G. Luo, H. Y. Nan, H. Guo, P. Wang, L. L. Zhang, M. M. Zhou, Z. Y. Yang, Y. Shi, W. D. Hu, Z. H. Ni, T. Qiu, Z. F. Yu, J. B. Xu, X. R. Wang, *Adv. Mater.* **2016**, 28, 5200.

[24] B. Wu, Y. H. Zhao, H. Y. Nan, Z. Y. Yang, Y. H. Zhang, H. J. Zhao, D. W. He, Z. L. Jiang, X. L. Liu, Y. Li, Y. Shi, Z. H. Ni, J. L. Wang, J. B. Xu, X. R. Wang, *Nano Lett.* **2016**, 16, 3754.

[25] D. W. He, Y. M. Pan, H. Y. Nan, S. A. Gu, Z. Y. Yang, B. Wu, X. G. Luo, B. C. Xu, Y. H. Zhang, Y. Li, Z. H. Ni, B. G. Wang, J. Zhu, Y. Chai, Y. Shi, X. R. Wang, *Appl. Phys. Lett.* **2015**, 107, 183103.

[26] A. L. Briseno, S. C. B. Mannsfeld, M. M. Ling, S. H. Liu, R. J. Tseng, C. Reese, M. E. Roberts, Y. Yang, F. Wudl, Z. N. Bao, *Nature* **2006**, 444, 913.

[27] G. Giri, S. Park, M. Vosgueritchian, M. M. Shulaker, Z. N. Bao, *Adv. Mater.* **2014**, 26, 487.

[28] S. C. B. Mannsfeld, A. Sharei, S. H. Liu, M. E. Roberts, I. McCulloch, M. Heeney, Z. A. Bao, *Adv. Mater.* **2008**, 20, 4044.

[29] L. Ying, B. B. Y. Hsu, H. M. Zhan, G. C. Welch, P. Zalar, L. A. Perez, E. J. Kramer, T. Q. Nguyen, A. J. Heeger, W. Y. Wong, G. C. Bazan, *J. Am. Chem. Soc.* **2011**, 133, 18538.

[30] H. N. Tsao, D. M. Cho, I. Park, M. R. Hansen, A. Mavrinskiy, D. Y. Yoon, R. Graf, W. Pisula, H. W. Spiess, K. Mullen, *J. Am. Chem. Soc.* **2011**, 133, 2605.

[31] S. H. Wang, M. Kappl, I. Liebewirth, M. Muller, K. Kirchhoff, W. Pisula, K. Mullen, *Adv. Mater.* **2012**, 24, 417.

[32] C. Luo, A. K. K. Kyaw, L. A. Perez, S. Patel, M. Wang, B. Grimm, G. C. Bazan, E. J. Kramer, A. J. Heeger, *Nano Lett.* **2014**, 14, 2764.

[33] Y. C. Wu, J. G. Feng, B. Su, L. Jiang, *Adv. Mater.* **2016**, 28, 2266.

[34] J. G. Feng, X. X. Yan, Y. F. Zhang, X. D. Wang, Y. C. Wu, B. Su, H. B. Fu, L. Jiang, *Adv. Mater.* **2016**, 28, 3732.

[35] H. J. Shin, K. K. Kim, A. Benayad, S. M. Yoon, H. K. Park, I. S. Jung, M. H. Jin, H. K. Jeong, J. M. Kim, J. Y. Choi, Y. H. Lee, *Adv. Funct. Mater.* **2009**, 19, 1987.

[36] J. L. Bredas, J. P. Calbert, D. A. da Silva, J. Cornil, *P. Natl. Acad. Sci. USA* **2002**, 99, 5804.

[37] G. Giri, E. Verploegen, S. C. B. Mannsfeld, S. Atahan-Evrenk, D. H. Kim, S. Y. Lee, H. A. Becerril, A. Aspuru-Guzik, M. F. Toney, Z. A. Bao, *Nature* **2011**, 480, 504.

[38] G. Kresse, J. Furthmuller, *Phys. Rev. B* **1996**, 54, 11169.

[39] G. Kresse, D. Joubert, *Phys. Rev. B* **1999**, 59, 1758.

[40] Y. Zhao, D. G. Truhlar, *J. Chem. Phys.* **2006**, 125, 194101.

[41] B. Hajgato, S. Guryel, Y. Dauphin, J. M. Blairon, H. E. Miltner, G. Van Lier, F. De Proft, P. Geerlings, *J. Phys. Chem. C* **2012**, 116, 22608.

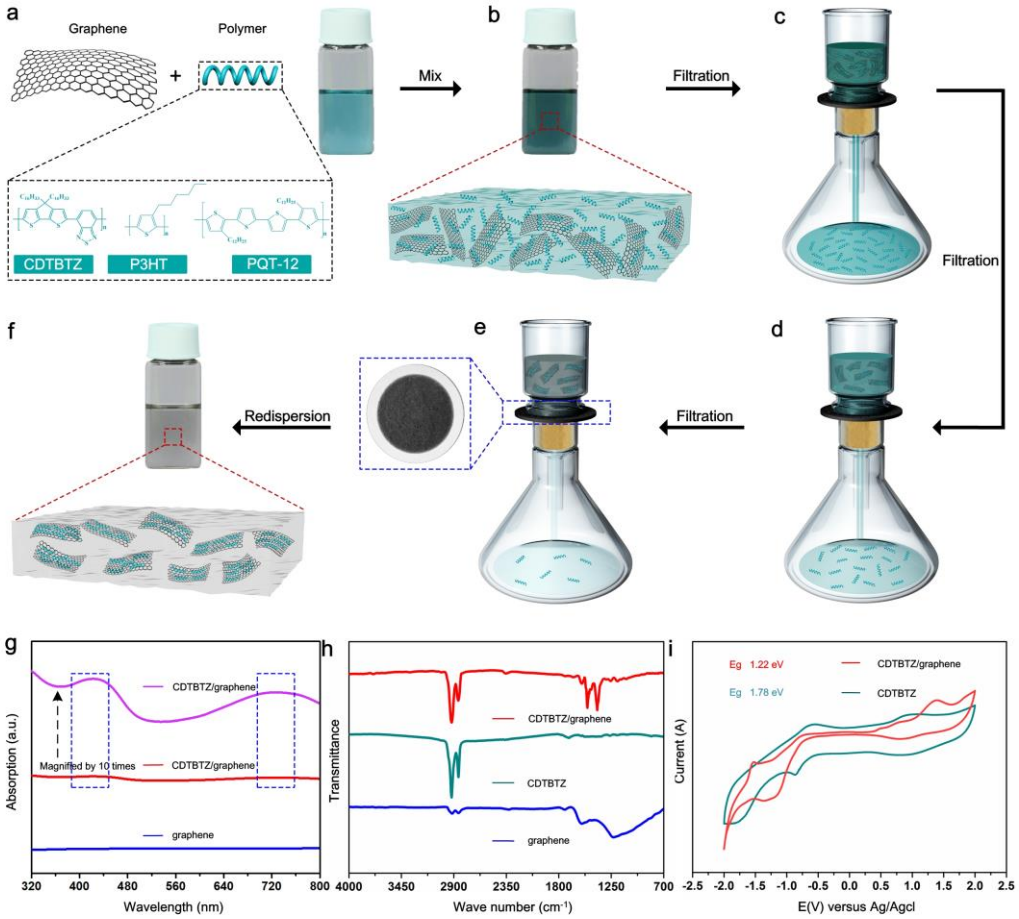

Figure 1. Methodology for the formation of π-conjugated polymer/graphene composite**.** a) The schematic illustration of graphene sheets and conjugated polymer. The molecular structures of three conjugated polymers are listed below. The clear blue liquid is the semiconductive polymer CDTBTZ dissolved into 1,2- dichlorobenzene. b) After the addition of graphene into the solution of polymer CDTBTZ, CDTBTZ can be adsorbed onto the graphene planes according to π-π interaction. The dark blue dispersion of CDTBTZ and graphene are showed on the right. c-e) After adsorption of conjugated polymer on the surface of the two-dimensional graphene sheets, filtration combined with drip washing were employed for ensurance of several-layer conjugated polymer on graphene. The inset on the right is a photo image of the polymer/graphene composite materials on a filter. f) The resulted powder (π-conjugated polymer/graphene composite materials) can be redispersed homogeneously in organic solvent, providing possibility for solution assembly afterwards. g) UV-vis spectra of CDTBTZ/graphene composite and graphene, respectively. h) IR spectra of CDTBTZ/graphene composite, CDTBTZ and graphene, respectively. i) Cyclic voltammogram curves of CDTBTZ and CDTBTZ/graphene composite, showing the bandgaps of 1.78 eV and 1.22 eV, respectively.

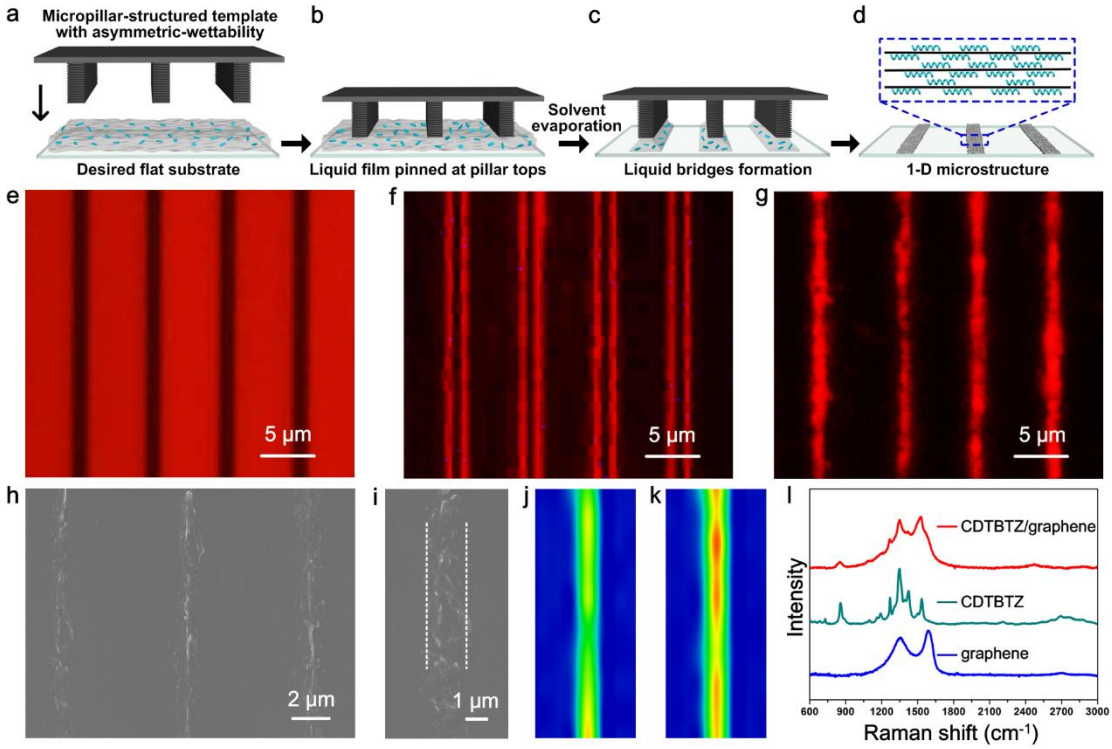

Figure 2. Mechanism and characterization of 1D CDTBTZ/graphene composite arrays. a) A "sandwich-shaped" assembly system was generated after dropping the dispersion of CDTBTZ/graphene composite materials onto the line-pillar-structured silicon substrate with asymmetric wettability and covering a flat substrate. b) A continuous liquid film sandwiched between the flat substrate and micropillar-structured template. c) Formation of individual capillary bridges pinned onto the tops of micropillars. d) 1D arrays of polymer/graphene composite with controlled position and alignment fabricated onto the target substrate after the total evaporation of the solvent. The figure on top shows the layer by layer configuration of polymer/graphene composite materials. e-g) Top-view microscopy images of the whole dewetting process observed from the dark-field. h) SEM image of the patterned 1D structures with uniform and precise position, the gaps between neighboring 1D stripes are homogeneous with ca. 5 μm. i) Magnified SEM image of an individual stripe, showing wrinkled and crumpled surface morphology. Raman mapping images of j) CDTBTZ adsorbed on graphene and k) graphene observed from 1D structures of CDTBTZ/graphene composite. l) Raman spectra of CDTBTZ/graphene composite, CDTBTZ and graphene, respectively.

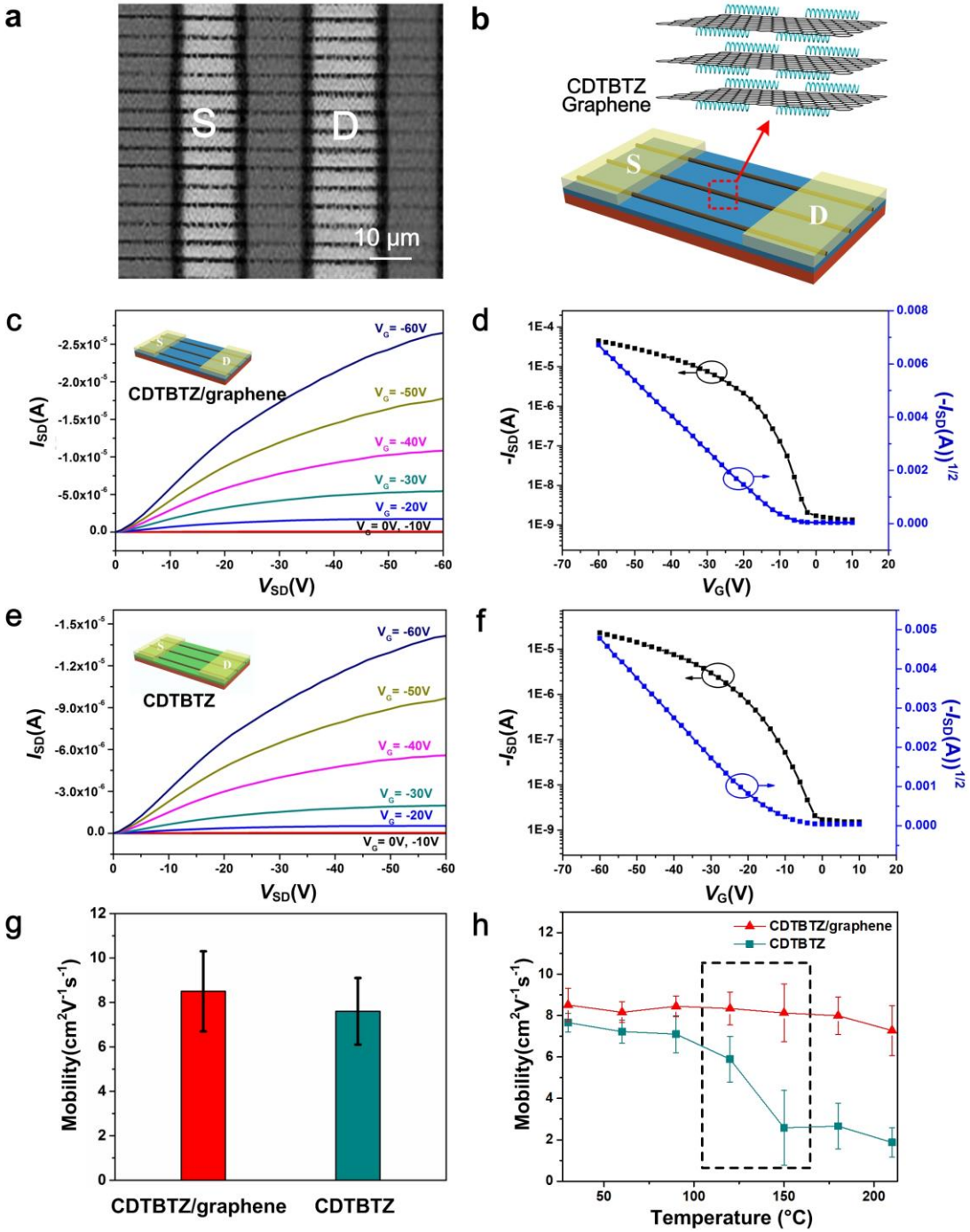

Figure 3. Fabrication of 1D arrays based organic field effect transistors (OFETs). a) Optical image of 1D polymer/graphene composite arrays contacted with the gold electrodes. b) Schematic diagram of OFETs with configuration of bottom gate and top contact. The as-prepared 1D structures are composed of conjugated polymer and graphene with a layer by layer conformation. c, d) Representative transfer and output curves of 1D CDTBTZ/graphene composite arrays. Inset in c shows the schematic diagram of OFETs based on 1D CDTBTZ/graphene composite arrays. e, f) Representative transfer and output curves of 1D CDTBTZ arrays. Inset in e shows the schematic diagram of OFETs based on 1D CDTBTZ arrays. g) Summary of the average hole mobilities calculated from 50 OFETs fabricated by 1D CDTBTZ/graphene composite arrays and 1D CDTBTZ arrays, respectively. h) Temperature-dependent mobility of devices based on CDTBTZ-graphene conjugated molecules and CDTBTZ molecules, respectively.

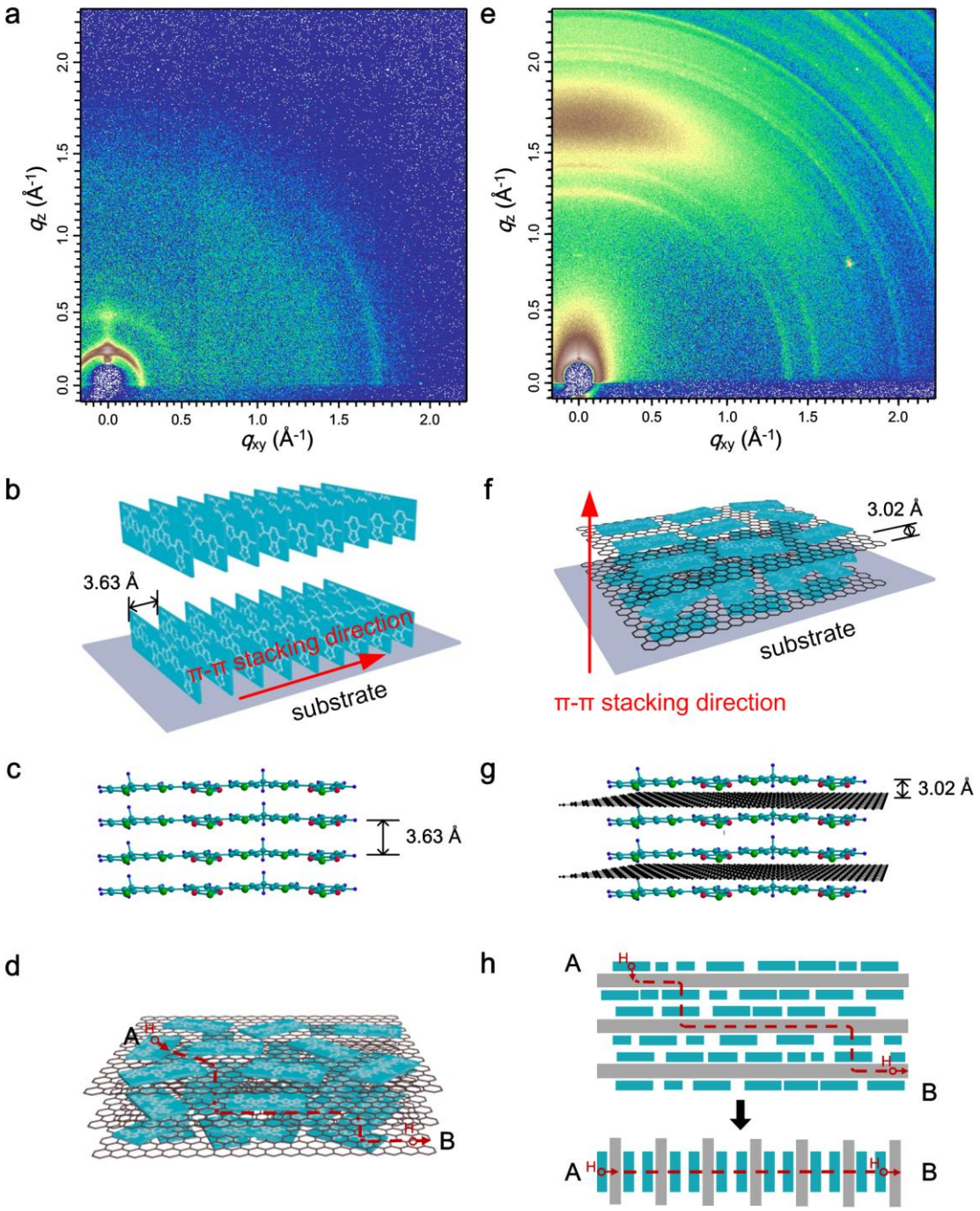

Figure 4. GIWAXS characterization of π-π stacking distance and molecular orientation. a) GIWAXS images of 1D CDTBTZ arrays. b) Schematic diagram of the possible molecular packing in the polymer-polymer system with the π-π stacking direction predominantly parallel to the substrate. c) The energy-minimized molecular structure of polymer dimer from the direction perpendicular to the thiophene ring plane, showing the π-π stacking distance. d) Primary charge transport route in polymer-graphene conjugated system. e) GIWAXS images of 1D CDTBTZ/graphene composite arrays. f) Schematic diagram of the possible molecular packing in the polymer-graphene conjugated system with the π-π stacking direction predominantly perpendicular to the substrate. g) The energy-minimized molecular structure of polymer dimer adsorbed on graphene from the direction perpendicular to the thiophene ring plane, showing the π-π stacking distance. h) The equivalent circuit of polymer-graphene conjugated system based field effect transistor.

***π*-conjugated polymer/graphene composite arrays** have been constructed for enhancing the charge-carrier transport and thermal stability with a low polymer consumption. By employing an asymmetric-wettability assembly system, the composite material is deterministically integrated into one-dimensional arrays for scale-up fabrication of field-effect transistors. Owing to the strong *π*-*π* interaction, charge transfer from conjugated polymers to graphene provides an efficient pathway for carrier transport and realization of high mobility.

Keywords: *π*-*π* interaction, organic semiconductors, graphene, solution adsorption, field-effect-transistors

Yun Liu, Wei Hao, Huiying Yao, Jia Zhu, Shuzhou Li, Yuchen Wu*, Lei Jiang*

Solution adsorption formation of a *π*-conjugated polymer/graphene composite for high-performance field effect transistors

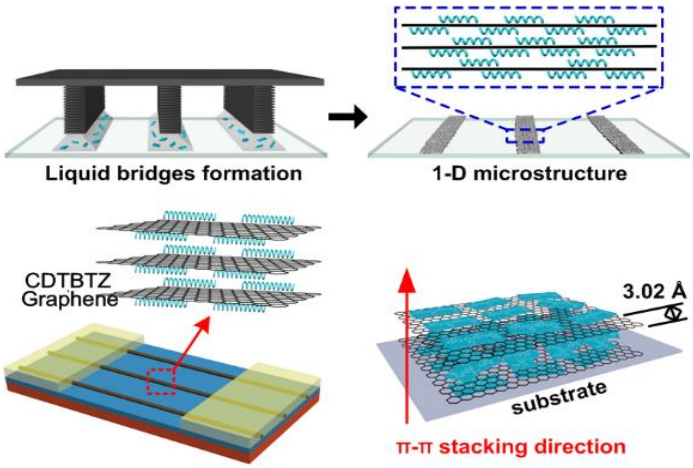

Supporting Information

Solution adsorption formation of a π-conjugated polymer/graphene composite for high-performance field effect transistors

Yun Liu, Wei Hao, Huiying Yao, Jia Zhu, Shuzhou Li, Yuchen Wu, Lei Jiang**

Dr. Y. Liu
Beijing National Laboratory for Molecular Sciences (BNLMS), Key Laboratory of Green Printing, Institute of Chemistry, Chinese Academy of Sciences, Beijing 100190, P. R. China

Dr. Y. C. Wu, Prof. L. Jiang
Key Laboratory of Bio-inspired Materials and Interfacial Science, Technical Institute of Physics and Chemistry, Chinese Academy of Sciences, Beijing 100190, China. Email: wuyuchen@iccas.ac.cn, jianglei@iccas.ac.cn

Dr. H. Y. Yao, Prof. J. Zhu
Department of Chemistry, Beijing Normal University, Beijing 100875, China.

Dr. W. Hao, Prof. S. Z. Li
School of Material Science and Engineering, Nanyang Technological University, Singapore 639798.

Prof. L. Jiang
School of Chemistry and Environment, Beihang University, Beijing 100191, China.

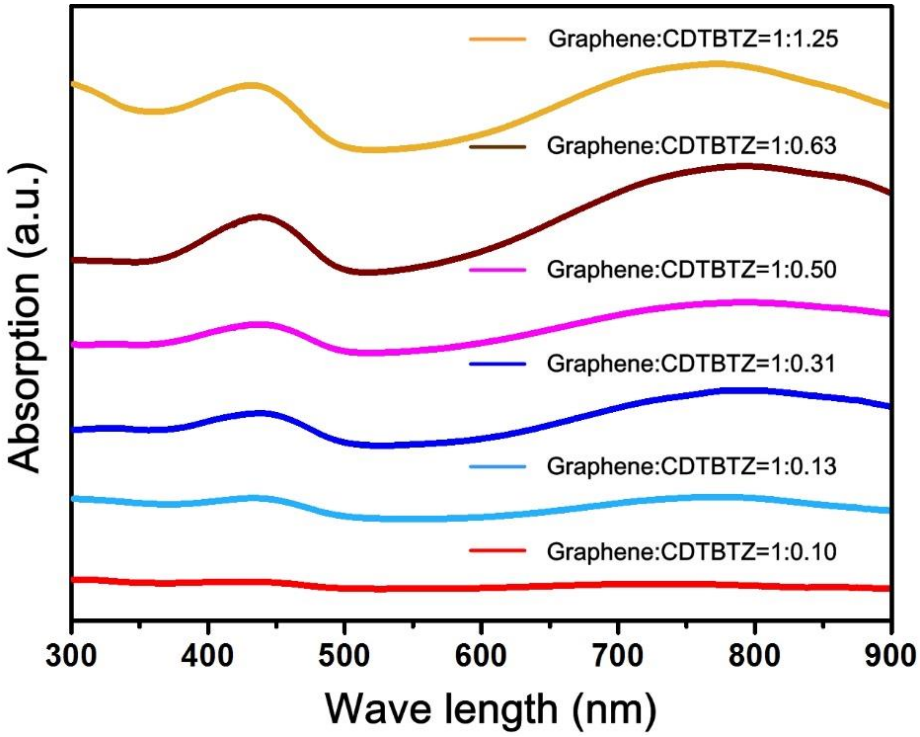

Figure S1. UV-vis absorption spectra of CDTBTZ/graphene composite membrane. The intensity of the absorption spectrum varies with the mass ratio of graphene and CDTBTZ in the CDTBTZ/graphene composite membrane. Following the time of vacuum filtration and washing with solvents increases, the quantity of CDTBTZ adsorbed on graphene decrease, generating decreased intensity of the UV-vis absorption spectrum accordingly. When the mass ratio of graphene and CDTBTZ is ca. 1:0.1, the UV-vis absorption intensity do not decrease, indicating that the relative amount of polymer CDTBTZ adsorbed on graphene through π-π interaction.

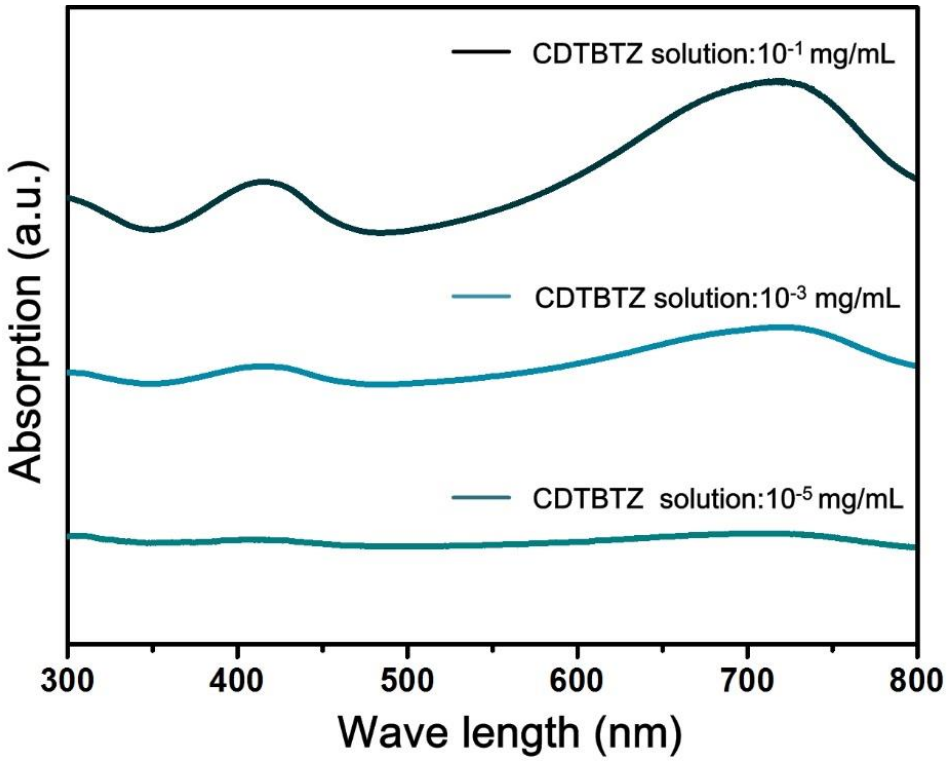

Figure S2. UV-vis absorption spectra of CDTBTZ solution with different concentrations. As the concentration of CDTBTZ solution decreases, the intensity of the UV-vis absorption spectrum decrease accordingly without change of peak number.

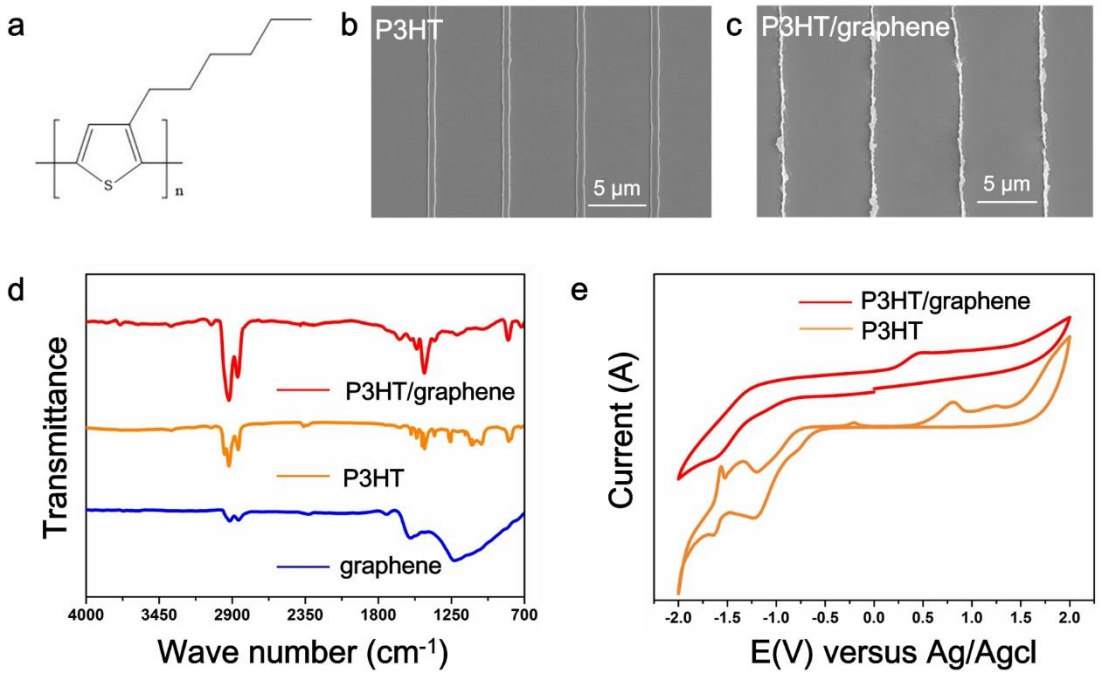

Figure S3. Precise positioning of 1D structures of P3HT/graphene composite. a) Molecular structure of poly-(3-hexylthiophene) (P3HT). b, c) Top view SEM image of the patterned 1D arrays of P3HT and P3HT/graphene composite, respectively. d) Micro-FTIR spectra of P3HT/graphene composite, P3HT and graphene. e) Cyclic voltammogram curves of P3HT and P3HT/graphene composite.

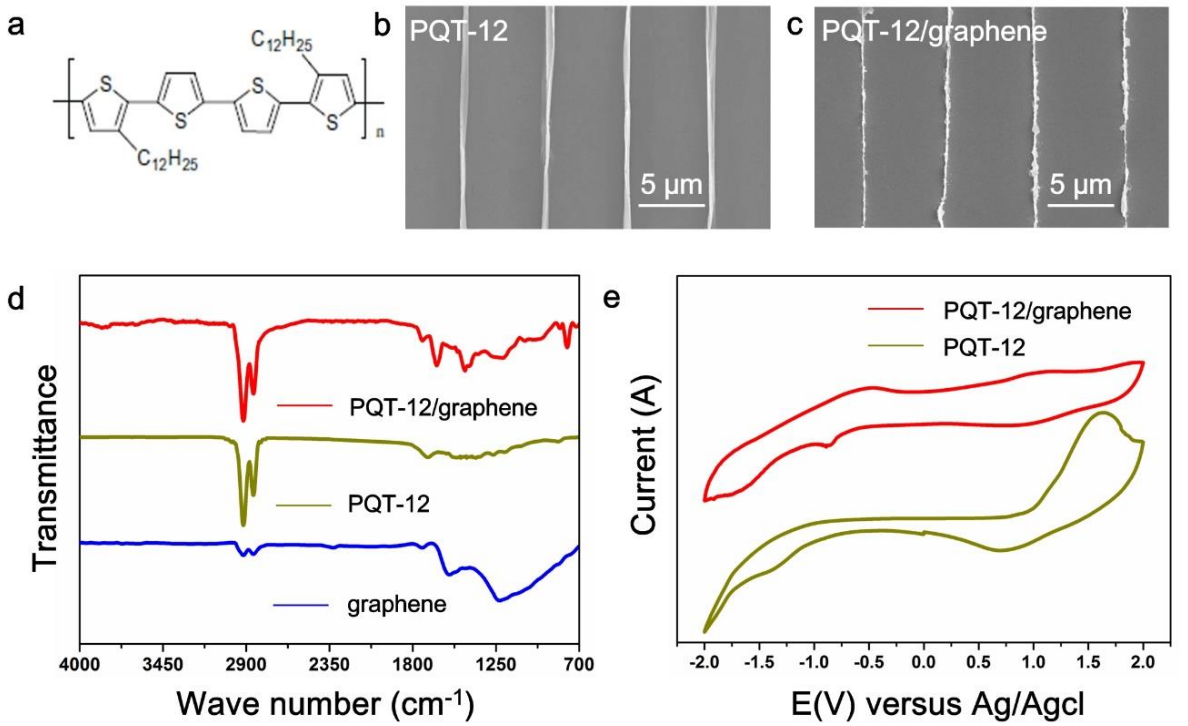

Figure S4. Precise positioning of 1D structures of PQT-12/graphene composite. a) Molecular structure of poly (3,3-didodecylquaterthiophene) (PQT-12). b, c) Top view SEM image of the patterned 1D arrays of PQT-12 and PQT-12/graphene composite, respectively. d) Micro-FTIR spectra of PQT-12/graphene composite, PQT-12 and graphene. e) Cyclic voltammogram curves of PQT-12 and PQT-12/graphene composite.

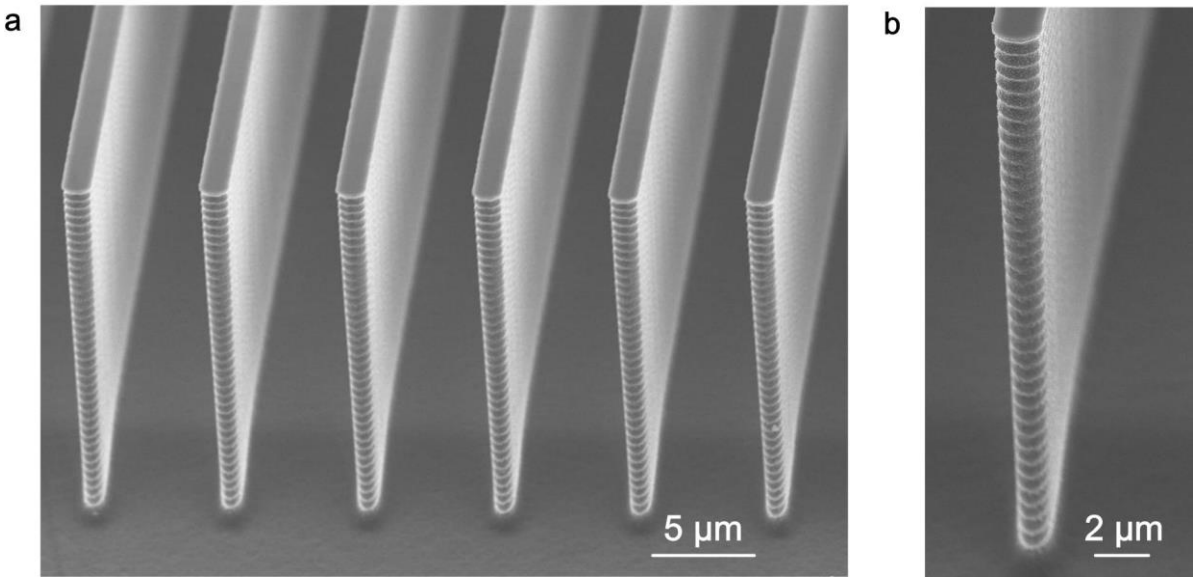

Figure S5. Template used to guide the fabrication process in this study. a) Scanning electron microscope (SEM) investigation of the line-pillar-structured template with the width of 2 µm, separation of 5 µm and depth of 20 µm. b) Magnified SEM observation of an individual micropillar.

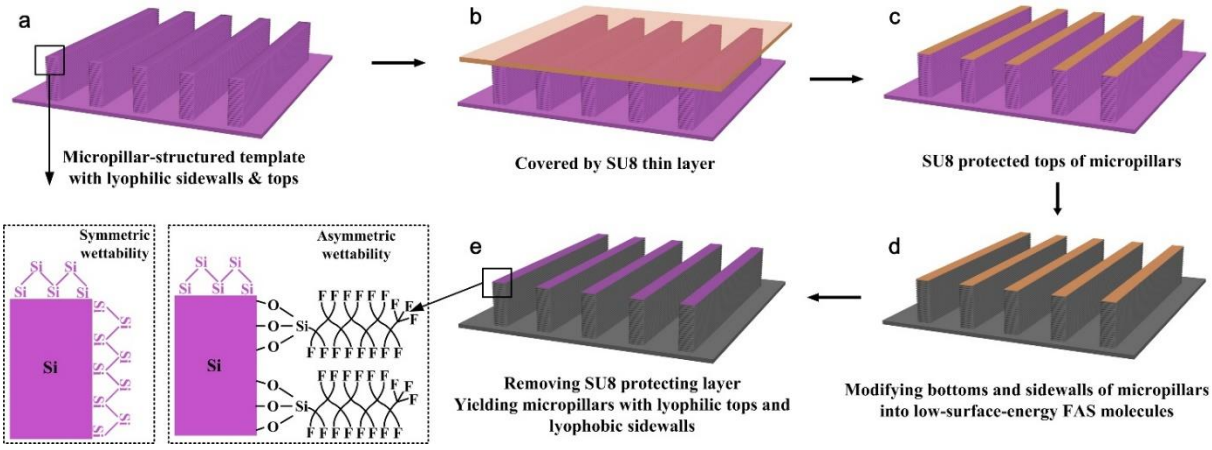

Figure S6. Schematic illustration of asymmetric-wettability modification to generate micropillars with lyophilic tops and lyophobic sidewalls. a) Symmetric wettability with lyophilic sidewalls and tops of micropillar-structured template at the preliminary states. b) The selective modification of micropillars was realized by covering a flat substrate to protect the tops of micropillars. In detail, the flat substrate was coated with a thin layer of SU8 film followed by pressing it onto the micropillar-structured template. c) The SU8 thin layer was covered onto the tops of micropillars after peeling off the flat substrate and baking. d) The top-protected micropillar-structured template was modified by heptadecafluorodecyl-trimethoxysilane (FAS) molecules with low surface energy in a decompression environment at room temperature for 24h and then heated at 80 ^{o}C for 3h. e) After removing the SU8 protection layer by acetone, the asymmetric-wettability of micropillars with lyophilic tops and lyophobic sidewalls were fabricated.

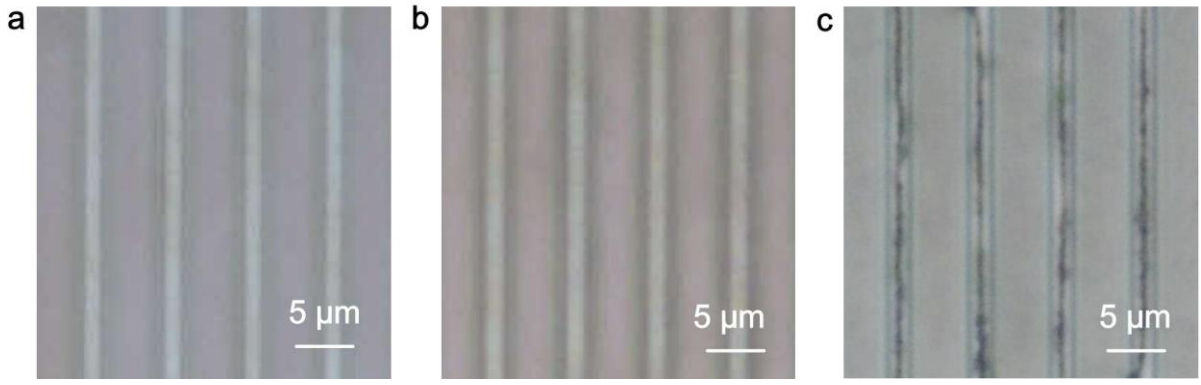

Figure S7. 1D arrays can be obtained through a capillary-bridge mediated assembly technique. a-c) Top-view microscopy images of the whole dewetting process observed from the bright-field.

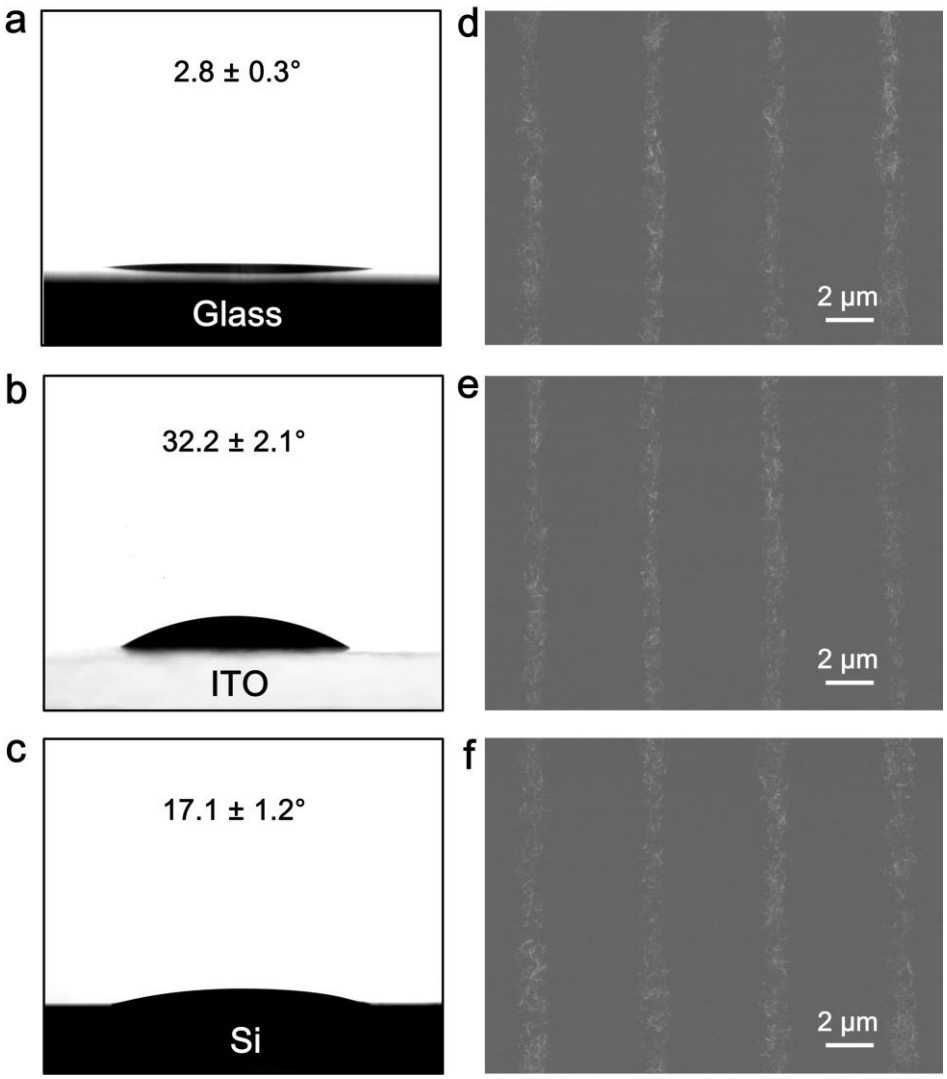

Figure S8. Contact angle of DMF on a) glass, b) ITO, c) Si substrates. Representative SEM images of the successfully assembled 1D polymer/graphene composite arrays on d) glass, e) ITO, f) Si substrates.

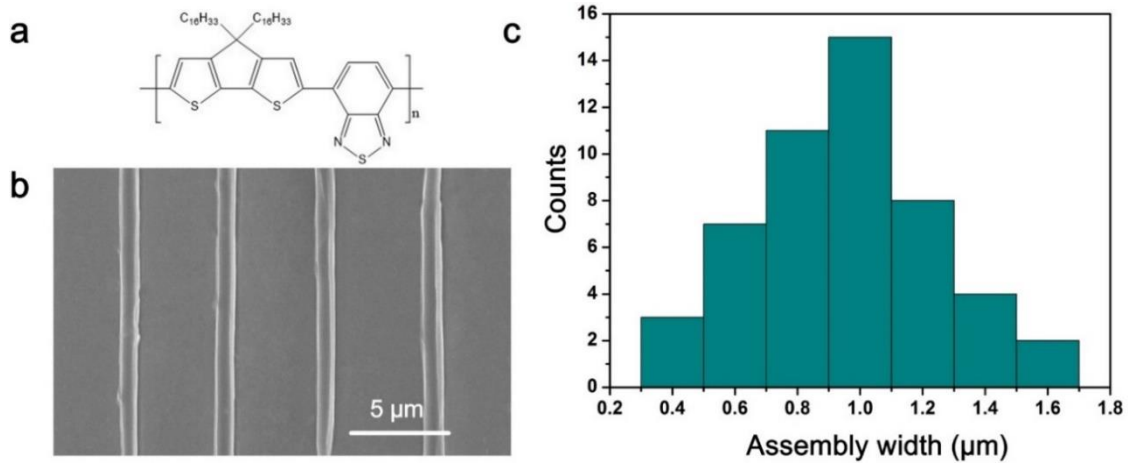

Figure S9. Regular and uniform 1D polymer arrays fabricated through the process. a) Molecular structure of poly[2,6-(4,4-bis-alkyl-4H-cyclopenta-[2,1-b;3,4-b0]-dithiophene)-alt-4,7-(2,1,3-enzothiadiazole)] (cyclopentadithiophene-benzothiadiazole; CDTBTZ). b) Top view SEM image of the as-prepared 1D CDTBTZ arrays, showing regular linear architectures towards one direction at equal spacing. c) Assembly width of the as-prepared 1D CDTBTZ arrays collected from 50 samples and the average width is 950±160 nm, suggesting the narrow size distribution of the 1D structures.

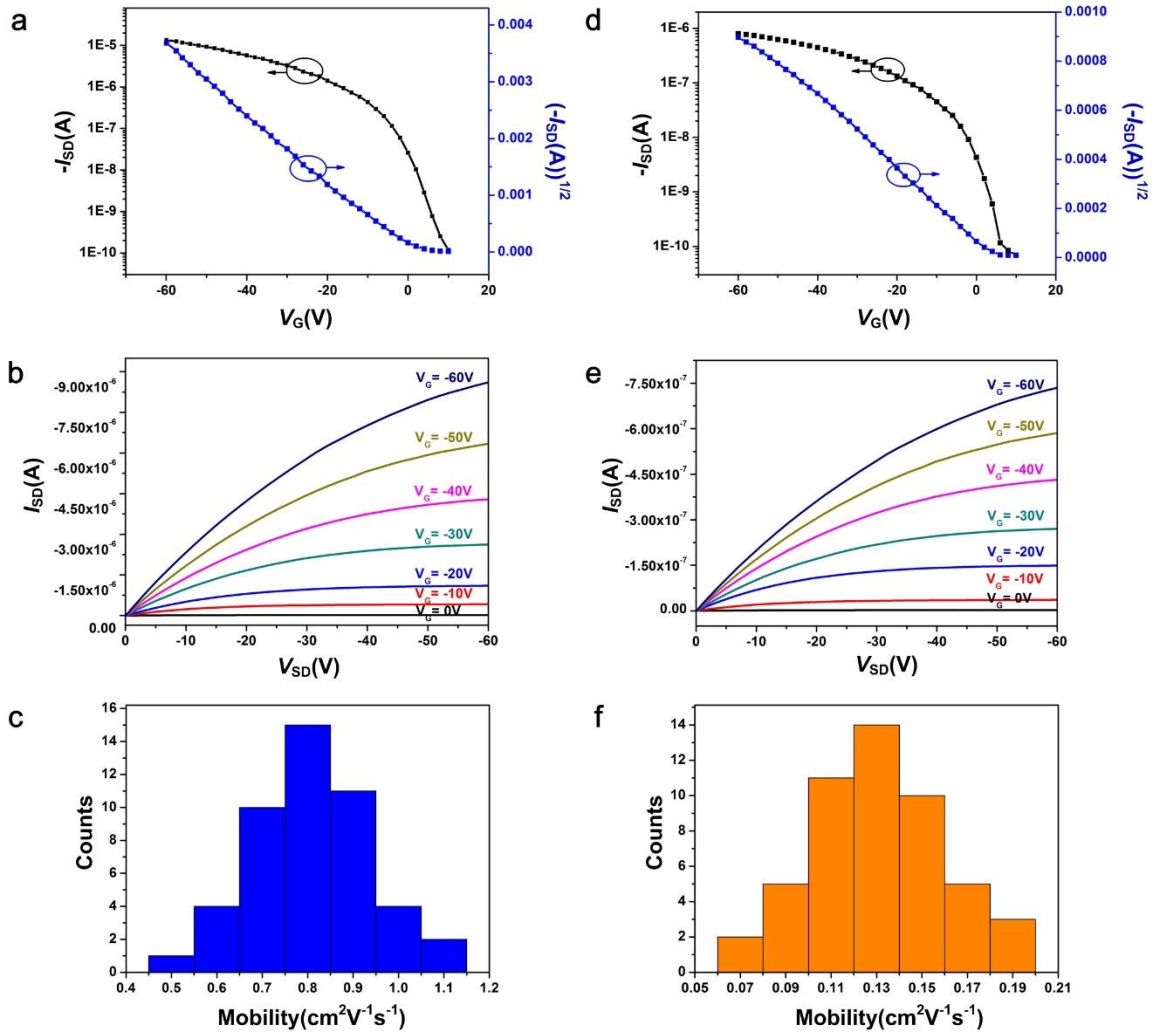

Figure S10. Improved performance of OFETs based on 1D P3HT/graphene composite arrays when compared with that based on 1D P3HT arrays. a, b) Representative transfer and output curves of 1D P3HT/graphene composite arrays, exhibiting an average hole mobility of 0.82 $cm^2V^{-1}s^{-1}$ (range from 0.47 to 1.13 $cm^2V^{-1}s^{-1}$) and on-to-off current ratio of 10^5. c) Histograms of hole mobility calculated from 50 OFETs fabricated by 1D P3HT/graphene composite arrays. d, e) Representative transfer and output curves of 1D P3HT arrays, exhibiting an average hole mobility of 0.13 $cm^2V^{-1}s^{-1}$ (range from 0.07 to 0.19 $cm^2V^{-1}s^{-1}$) and on-to-off current ratio of 10^4. f) Histograms of hole mobility calculated from 50 OFETs fabricated by 1D P3HT arrays.

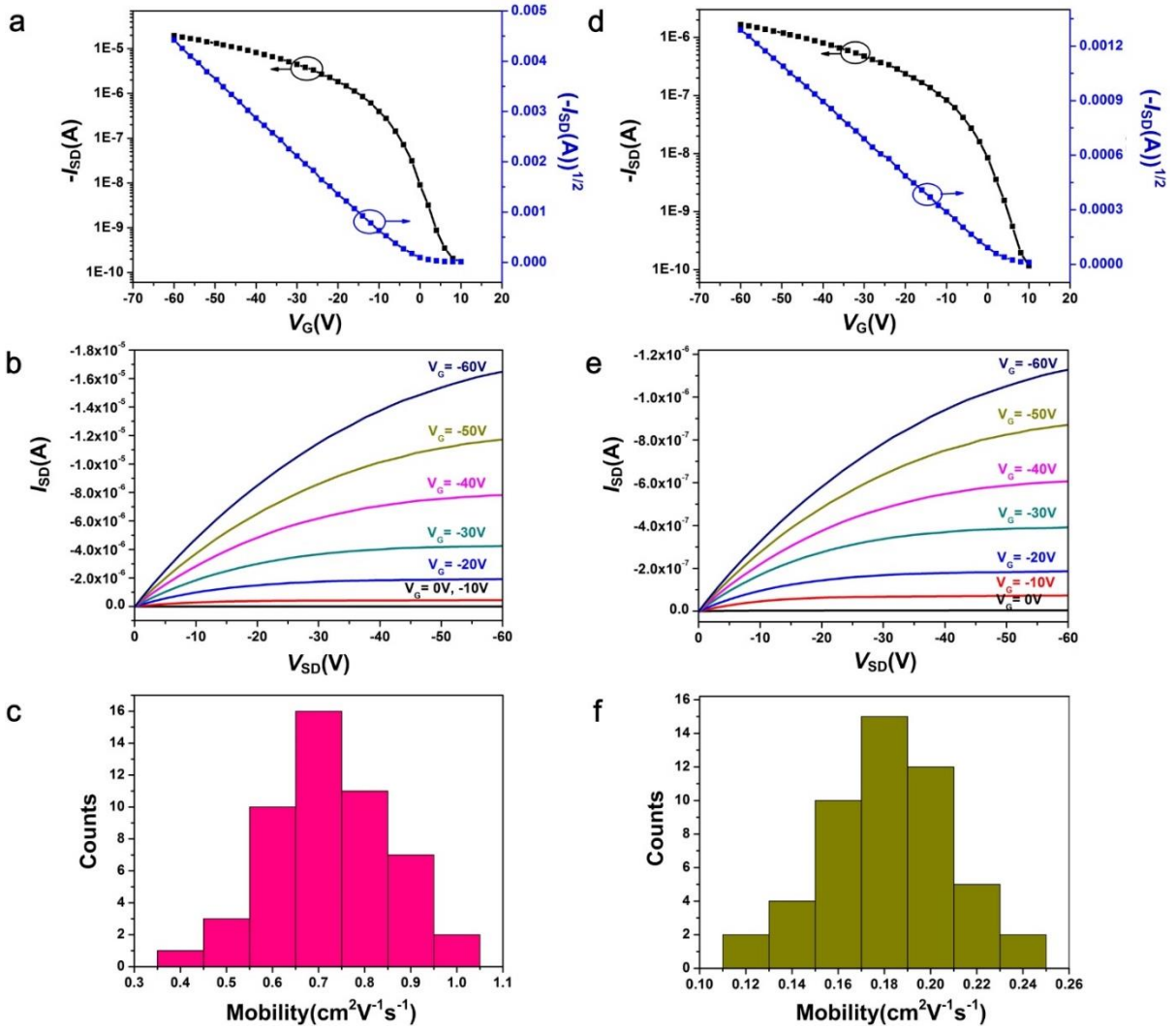

Figure S11. Improved performance of OFETs based on 1D PQT-12/graphene composite arrays when compared with that based on 1D PQT-12 arrays. a, b) Representative transfer and output curves of 1D PQT-12/graphene composite arrays, exhibiting an average hole mobility of 0.73 $cm^2V^{-1}s^{-1}$ (range from 0.42 to 1.05 $cm^2V^{-1}s^{-1}$) and on-to-off current ratio of 10^5. c) Histograms of hole mobility calculated from 50 OFETs fabricated by 1D PQT-12/graphene composite arrays. d, e) Representative transfer and output curves of 1D PQT-12 arrays, exhibiting an average hole mobility of 0.18 $cm^2V^{-1}s^{-1}$ (range from 0.12 to 0.24 $cm^2V^{-1}s^{-1}$) and on-to-off current ratio of 10^4. f) Histograms of hole mobility calculated from 50 OFETs fabricated by 1D PQT-12 arrays.

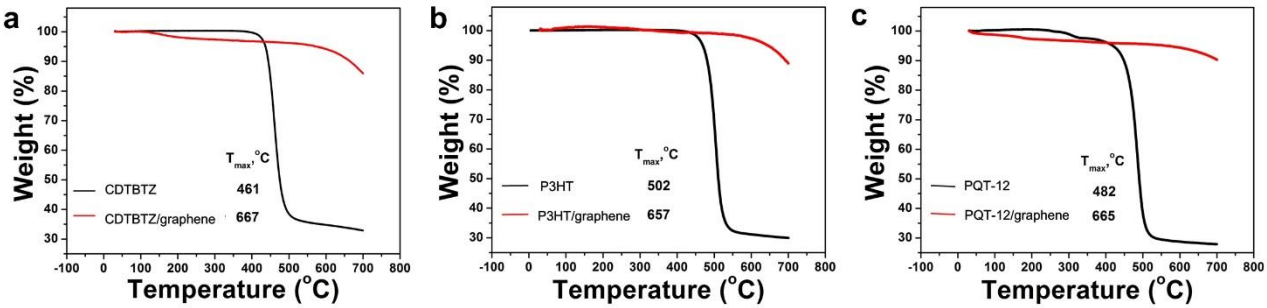

Figure S12. Thermogravimetric analysis (TGA) curves of polymers and conjugated polymer/graphene composite. T_{max} represents the temperature of maximum mass loss rate. a) TGA curves of CDTBTZ and CDTBTZ/graphene composite, showing enhanced thermal stability by the conjugation with graphene as T_{max} shifts toward higher temperature. The total mass loss are 67% and 14%, respectively. b) TGA curves of P3HT and P3HT/graphene composite, exhibiting T_{max} of 502 ^{o}C and 657 ^{o}C, respectively. When the temperature reaches 700 ^{o}C, the mass loss are 70% and 11%, respectively. c) TGA curves of PQT-12 and PQT-12/graphene composite, exhibiting T_{max} of 482 ^{o}C and 665 ^{o}C, respectively. When the temperature reaches 700 ^{o}C, the mass loss are 72% and 10%, respectively.

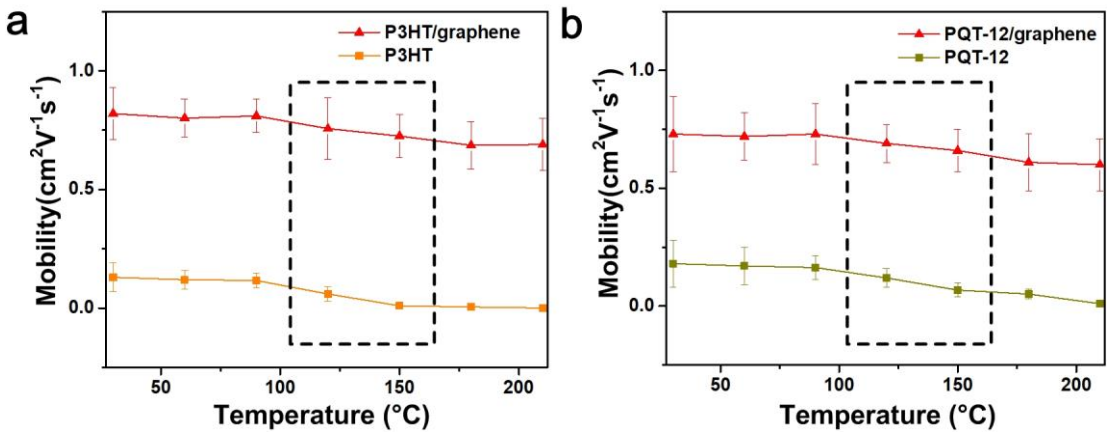

Figure S13. Temperature-dependent mobility of devices based on a) P3HT-graphene conjugated molecules and P3HT molecules, b) PQT-12-graphene conjugated molecules and PQT-12 molecules, respectively.

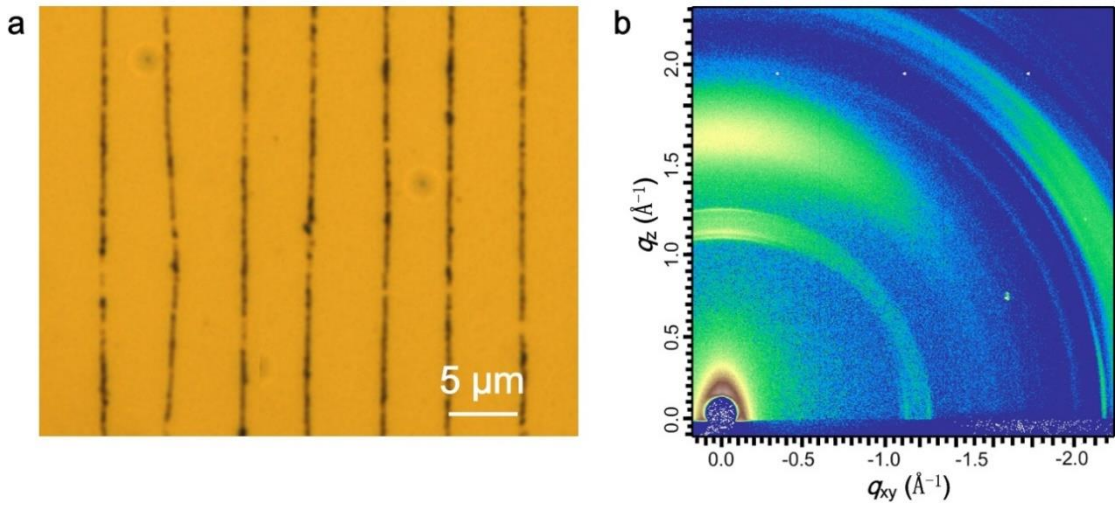

Figure S14. Large area of regular and uniform 1D arrays of graphene. a) Top view microscopy image of the as-prepared 1D graphene arrays with regular linear architectures at equal spacing. b) GIWAXS images of 1D graphene arrays, showing an interlayer distance of 3.83 Å, which was determined from the high-order scattering in the out-of-plane axis at q ~ 1.64 Å^{-1}.

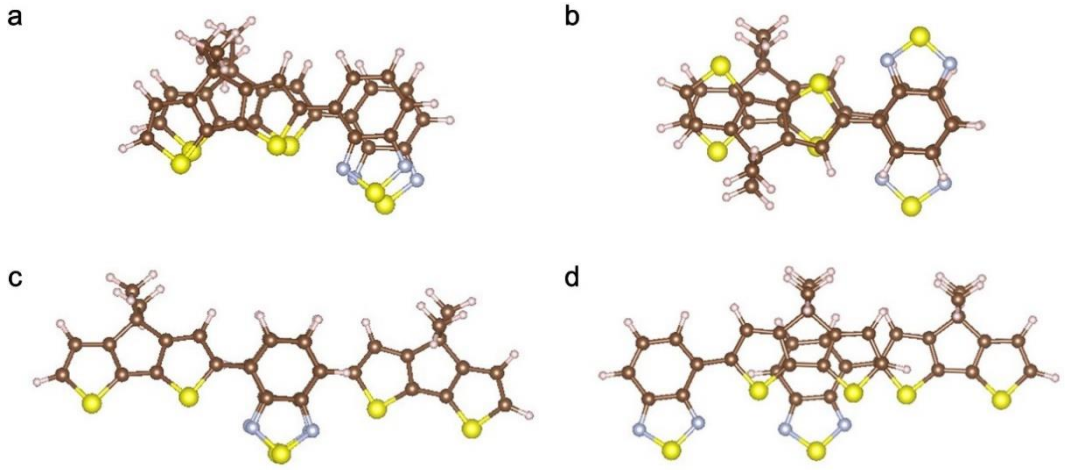

Figure S15. Top view of the studied four configurations of CDTBTZ-methyl dimer optimised by density functional theory (DFT) that implanted in Vienna ab initio simulation package (VASP). Yellow: S, brown: C, light blue: N, white: H. a) Cofacial configuration with methyl on the same side. b) Inverted Cofacial configuration with methyl on different sides. c) A2A staggered configuration. (d) A2D staggered configuration. The binding energy of a-d) is 0.512 eV, 0.564 eV, 0.332 eV and 0.293 eV, respectively, indicating the inverted cofacial configuration is the most stable one. The average and minimum distances in CDTBTZ-methyl dimer with inverted cofacial configuration are 3.396 Å and 3.286 Å, respectively.

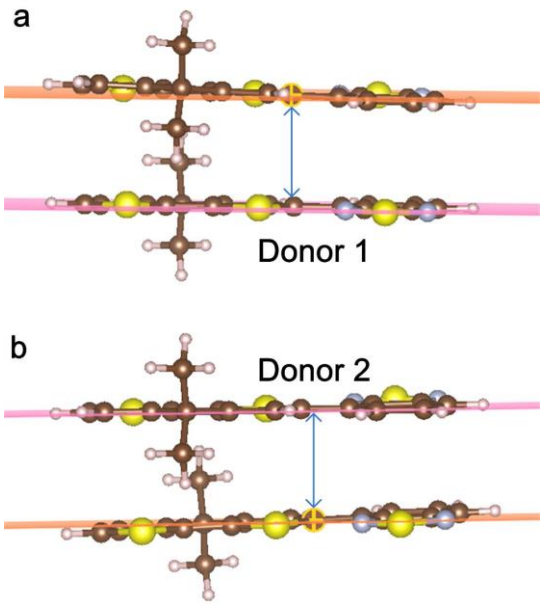

Figure S16. Calculation method for π-π stacking distance. For CDTBTZ-methyl dimer, we calculated the average distances of acceptor-to-acceptor and donor-to-donor respectively in the first stage, then the two distances were averaged again to be the π-π stacking distance. Set the calculation of the average distance of donor-to-donor in CDTBTZ-methyl dimer as an example. Firstly donor1 was selected as base plane (pink one in Figure S12a) and average distances of all atoms in the other donor was computed. Secondly the same method was used to calculate distances in donor2 (pink one in Figure S12b). Average distance is the average value of two averages obtained in the first and second step.

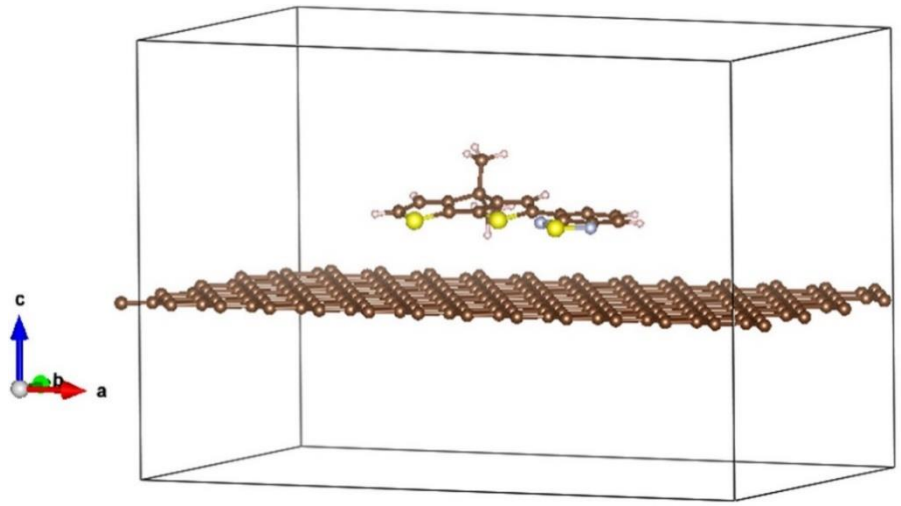

Figure S17. The optimized configuration of CDTBTZ monomer/graphene composite optimised by density functional theory (DFT) that implanted in Vienna ab initio simulation package (VASP). The average and minimum distances in CDTBTZ monomer/graphene composite are 3.399 Å and 3.122 Å, respectively. The binding energy of CDTBTZ-methyl monomer adsorbed on graphene is calculated to be 0.770 eV, which is much stronger than that of CDTBTZ-methyl dimer.

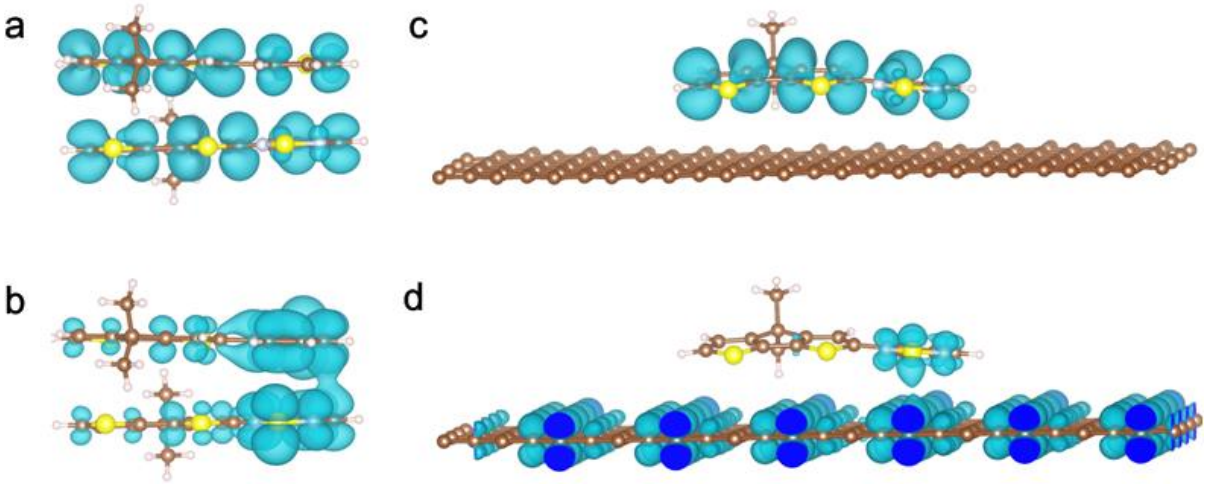

Figure S18. Electronic energy levels of polymers and conjugated polymer/graphene composites. a) HOMO and b) LUMO diagrams of CDTBTZ dimer calculated by DFT theory, the band gap energy is calculated to be 1.499 eV. c) HUMO and d) LUMO diagrams of CDTBTZ/graphene composite calculated by DFT theory, the band gap energy is calculated to be 0.956 eV.

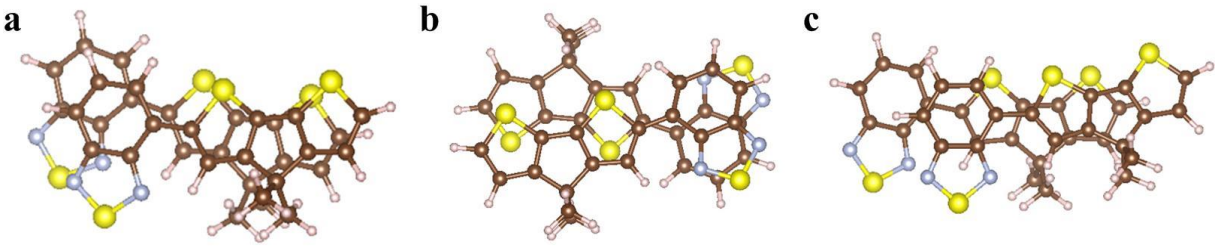

Figure S19. Top view of the studied three configurations of CDTBTZ-methyl dimer optimized by density functional theory (DFT) in the Gaussian09 program package based on M06L functional combined with 6-31G d). Yellow: S, brown: C, light blue: N, white: H. a) Cofacial configuration with methyl on the same side. b) Inverted Cofacial configuration with methyl on different sides. c) Staggered configuration with methyl on the same side. We adopted counterpoise correction of Boys and Bernardi[1] to minimize the basis set superpositon error (BSSE) in calculating binding energies. The binding energy of a-c) is 0.541 eV, 0.555 eV and 0.541 Ev, respectively, indicating the inverted cofacial configuration with methyl on different sides is the most stable configuration. The average and minimum distances in CDTBTZ-methyl dimer with inverted cofacial configuration are 3.452 Å and 3.325 Å, respectively.

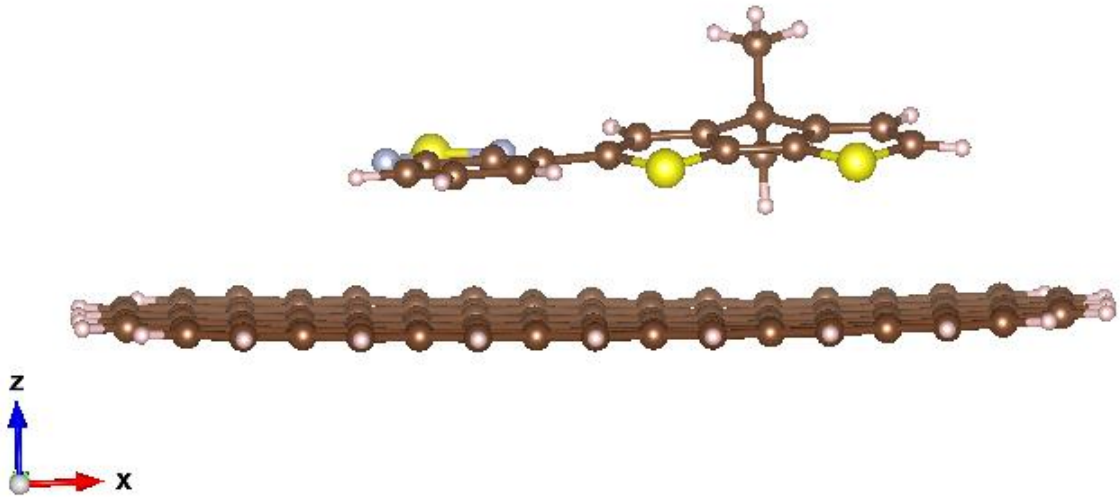

Figure S20. The optimized configuration of CDTBTZ monomer/graphene composite optimized by density functional theory (DFT) in the Gaussian09 program package based on M06L functional combined with 6-31G (d). The average and minimum distances in CDTBTZ monomer/graphene composite are 3.505 Å and 3.198 Å, respectively. The binding energy of CDTBTZ-methyl monomer adsorbed on graphene is calculated to be 0.812 eV, which is much stronger than that of CDTBTZ-methyl dimer.

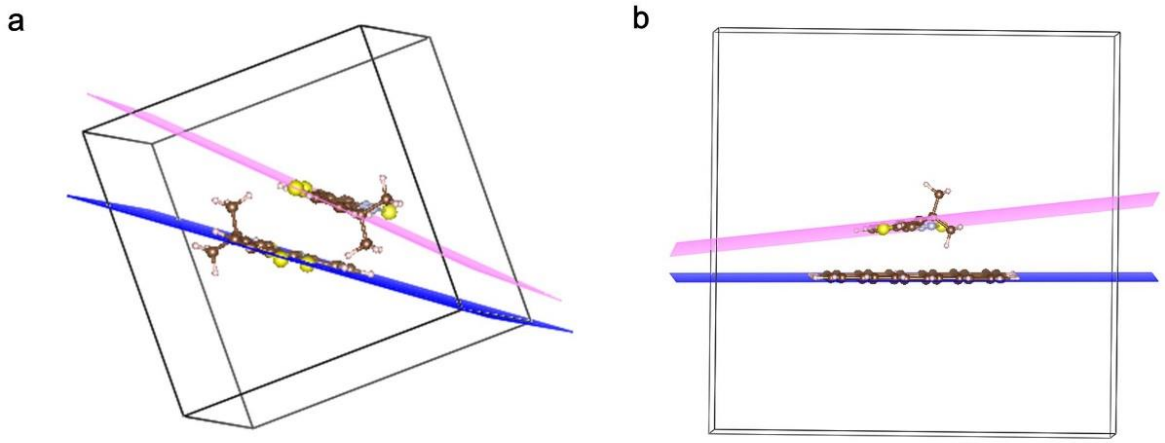

Figure S21. Side view of planes in CDTBTZ-methyl dimer and CDTBTZ monomer/graphene composite after optimization. The angle between two planes in CDTBTZ-methyl dimer a) is 8.506° and in CDTBTZ monomer/graphene composite b) is 6.286°. Smaller angle between two planes reveals that CDTBTZ monomer/graphene composite has better parallelism than dimer, which makes tighter π-π interaction with graphene that do great benefit to faster mobility.

Table S1. The calculated band gap energies, binding energies and π-π stacking distances in CDTBTZ-methyl dimer with inverted cofacial configuration and CDTBTZ monomer/ graphene composite optimized by density functional theory (DFT) that implanted in Vienna ab initio simulation package (VASP).

	Band gap energy (eV)	Binding energy (eV)	Minimum distance (Å)	Average distance (Å)
CDTBTZ-methyl dimer	1.499	0.564	3.286	3.396
CDTBTZ/graphene composite	0.956	0.770	3.122	3.399

Table S2. The calculated band gap energies, binding energies and π-π stacking distances in CDTBTZ-methyl dimer with inverted cofacial configuration and CDTBTZ monomer/ graphene composite optimized by density functional theory (DFT) in the Gaussian09 program package based on M06L functional combined with 6-31G (d).

	Band gap energy (eV)	Binding energy (eV)	Minimum distance (Å)	Average distance (Å)
CDTBTZ-methyl dimer	1.550	0.555	3.325	3.452
CDTBTZ/graphene composite	0.128	0.812	3.198	3.505

[1] S. F. Boys, F. Bernardi, *Mol. Phys.* **2002**, 100, 65.